Chapter 8

Combustion and Emissions of a Diesel Engine Fueled with Diesel-Biodiesel-Ethanol Blends and Supplemented with Intake CO_2 Charge Dilution

Ho Tse

Additional information is available at the end of the chapter

http://dx.doi.org/10.5772/64470

Abstract

This study investigated the influence of a four-cylinder naturally aspirated direct-injection diesel engine fueled with diesel-biodiesel-ethanol blended (DBE) fuels tested at a steady state speed of 1800 rev/min under different engine loads, ethanol volume and intake carbon dioxide (CO_2) dilution ratios on engine performance, combustion characteristics, regulated gaseous emissions, and soot agglomerates. Overall, the experimental results indicate that DBE blends can in general improve brake thermal efficiency (BTE) and reduce nitrogen oxides (NO_x), carbon monoxide (CO), CO_2, volatile organic fractions, particulate mass (PM), and particulate number (PN) concentrations, while brake-specific fuel consumption (BSFC) and hydrocarbon (HC) might increase slightly. Compared with ultra-low-sulfur diesel, DBE blends can maintain a good tradeoff relationship among PM-PN-NO_x. Compared with biodiesel, the blended fuels perform better in suppressing brake-specific particle number emissions (BSPN), leading to a reduction of ultrafine and nanoparticle numbers. The combined effect of DBE blends with intake CO_2 dilution has marginal effects on BSFC and BTE, significantly reducing NO_x emission while slightly increasing particulate emissions. On particulate characteristics, DBE blends produce soots with curved, tortuous, and disorganized nanostructures with low soot burnout temperature and strong oxidation rate favoring PM-PN reduction.

Keywords: diesel-biodiesel-ethanol, combustion characteristics, gaseous emissions, particle emissions, particle morphology

1. Introduction

1.1. Transport biofuels

The trend toward low-emission diesel fuels is growing worldwide with particular concerns from the regulated tradeoff emissions of NO_x and PM, and other air toxics. European Union (EU) mandates 10% share for biofuels in the EU total energy mix by 2020 and United States sets a total of 36 billion gallon target for biofuel production by 2022. Therefore, oxygenated-type biofuel become popular to be used and blended with diesel for producing cleaner burning fuels. Many researchers explore methods to improve fuel quality by blending with oxygenated additives as coproducts [1]. The commonly used oxygenated additives are (a) ethanol, (b) acetoacetic esters and dicarboxylic acid esters, ethylene glycol monoacetate, (c) 2-hydroxy-rhyl esters, (d) diethylene glycol dimethyl ether, (e) sorbitan monooleate and polyoxyethylene sorbitan monomethyl ether, (f) ethanol and dimethyl ether, (g) dimethyl ether (DME), (h) dimethyl carbonate (DMC), (i) 1-octylamino-3-octyloxy-2-propanol and *N*-octyl nitamine, (j) methanol, and (k) a mixture of methanol and ethanol. In fact, there are only few literatures studying the effects of oxygenated additives in CI engine experiments. Among these additives, DME, DMC, ethanol, or methanol have been studied by few researches as effective additives to be applied as coproducts in CI engines. **Table 1** lists their major advantages and limitations from literature findings on gaseous emissions and **Table 2** lists their fuel properties [1, 2].

1.2. Food, energy, and environment trilemma

Of the alternative biofuels, the most widely investigated include biodiesel and ethanol [3–5]. These two fuels have clear emission advantages over diesel. However, some studies have raised the concern of "food versus fuel" arising from plant-based biodiesel and ethanol, which might be the main hurdle for commercialization [6]. In fact, the economic consequences of these biofuel expansions are mixed and there are still some issues that will influence the actual impacts on food costs that have not been accounted for. To counter the "food, energy, and environment trilemma", the development of these biofuels from nonfood sources (i.e., biodiesel from waste cooking oil, ethanol from cellulosic nonfood crops, etc.) can show great promise in reducing food commodities being utilized for biofuel production [7].

1.3. Investigation of DBE blends

Focus of many previous researches was placed on diesel-biodiesel blends on general diesel engine performance and emissions as the fundamental investigation due to the interest of biodiesel being low cost, less polluting, renewable nature, and high energy density against diesel [8]. The dominant trend could be found in most research cases [9–13] that diesel-biodiesel blends would decrease the full-load effective power, increase brake-specific fuel consumption, and maintain thermal efficiency. As for vehicular emissions, partial regulated air parameters (viz., smoke density, particulate mass concentration, CO, and aromatic hydrocarbon) and partial unregulated air toxics (viz., formaldehyde, 1,3-butadiene, toluene, and xylene) decreased. However, other partial regulated air parameters (viz., NO_x, NO_2 and nanoparticle) and air toxics (viz., acetaldehyde and benzene) increased instead.

http://dx.doi.org/10.5772/64470

Oxygenated additives	Advantages	Limitations
Dimethyl ether (DME)	A slight decrease of NO_x emissions with % DMC in blended fuel. Strong effect on smoke reduction.	Maximum blending concentration up to 25% into diesel fuel; otherwise significantly reduce the viscosity of final mixture.
Dimethyl carbonate (DMC)	A slight decrease of NO_x emissions with % DMC in blended fuel. Most effective at 5% DMC for reducing submicro and microsized particle emissions.	Slight increase of HC and CO, but can be resolved with DOC. Obvious increase in benzene, toluene, and *m*,*p*-xylene (BTX) emissions. Increase in fuel consumption or decrease in engine power due to lower calorific value of DMC.
Ethanol	Effective in reducing particulate mass at high engine load. Effective in reducing unregulated emission of formaldehyde, ethane, ethene, 1,3-butadiene, and BTX.	Lower cetane number. Increase in fuel consumption or decrease in engine power. Increase of NO_2 (toxic and highly reactive gas) is associated with the use of ethanol-ULSD blends having adverse influence on human health.
Methanol	Effective at a fumigation ratio of 0.1 for reducing NO_x and particulate mass concentration. Particle emitted under methanol fumigated engine are reduced under both low and medium engine loads. No increase in the number of nanosized particles and changes in geometrical mean diameter of emitted particles under low and medium engine loads.	Maximum fumigation ratio of 0.4 for avoiding engine knock. Marginal reduction in particle emission in high engine loads. Significant increase of HC and CO with increase of fumigation ratio of methanol, but can be resolved with DOC. Increase of NO_2 (toxic and highly reactive gas) is associated with the use of methanol having adverse influence on human health.

Table 1. Advantages and limitations for four oxygenated additives.

Due to the increases in public concerns about the environmental and health impacts from diesel-biodiesel blends, further development of using additional oxygenated-type fuel additives (viz., ethanol) to improve engine and emission performance flaws from diesel-biodiesel blends is significant and viable [14]. In fact, there are very few literatures studying the effects of diesel-biodiesel-ethanol (DBE) blends in diesel engine experiments and the impacts from these new blends are still not fully understood till date. For long-term environmental and public health protection, new forms of clean and economical oxygenated diesel blends fuel must be explored to progressively replace conventional mineral diesel. Ethanol is the type of alcohol made from renewable resources such as biomass from locally grown crops and even waste products such as waste paper, grass, and tree trimmings. They are also an alternative transportation fuel since it has properties allowing its use in existing diesel engines with minor hardware. Despite this, they are only used on a limited basis to fuel diesel engines

due to their respective problems in toxicity, corrosivity, miscibility with water, or immiscibility with diesel. However, they have higher octane number enduring higher compression ratios before engine starts knocking, thus giving diesel engine an ability to deliver more power efficiently and economically and to produce lesser CO, HC, and NO_x/NO_2 with higher heat of vaporization, thereby reducing peak temperature inside combustion chamber [2, 3].

Property	Euro V diesel	Biodiesel	Ethanol	Methanol	DME	DMC
Cetane number	52	51	6	<5	55–60	35–36
Lower heating value (MJ/kg)	42.5	37.5	28.4	19.7	28.43	15.78
Density (kg/m^3) at 20°C	840	871	786	792	668	1079
Viscosity (mPa S) at 40°C	2.4	4.6	1.2	0.59	–	0.63
Heat of evaporation (kJ/kg)	250–290	300	840	1178	410	369
Carbon content (%mass)	86.6	77.1	52.2	37.5	52.2	40
Hydrogen content (%mass)	13.4	12.1	13	12.5	13	6.7
Oxygen content (%mass)	0	10.8	34.8	50	34.8	53.3
Sulfur content (%mass)	<10	<10	0	0	<10	<10

Table 2. Properties of Euro V diesel, biodiesel, ethanol, methanol, DME, and DMC.

The use of ethanol on a limited basis in diesel-biodiesel blends can compensate the decreased octane caused by the presence of biodiesel in diesel fuel and produce lesser particulates and CO_2 due to the lower carbon-to-hydrogen ratio of these alcohols. On the one hand, the presence of biodiesel can act as stabilizer to stabilize the phase stability of diesel-biodiesel-ethanol in blend fuels. Therefore, more understanding for the long-term stable diesel-biodiesel-ethanol (DBE) blends in diesel engine application with improved engine and emission performance can be achieved.

1.4. Novelty and contributions

This chapter provides the following contributions in filling the knowledge gaps on using DBE blends as potential transport biofuels that the current literatures do not cover or rarely study.

- Simultaneous reduction in NO_x and PM is a challenging issue in diesel industry. The use of DBE blends is proven to attain the reduction of both pollutants without engine modification works. The combined effect of DBE blends with intake CO_2 charge dilution can even reduce NO_x emission significantly while minimizing the adverse impact on particulate emissions.
- Correlation equations formulated through curve-fitting process for predicting percentage change in NO_x, CO, and HC emissions. The predicted percentage change has been found to agree closely with that of experimental data at the 95% confidence level.
- Correlation between combustion characteristic parameters and the particulate emissions for DBE blends over a range of ethanol contents. The soot reduction by DBE blends is associated with its lower cetane number and higher latent heat of evaporation thereby leading to longer ignition delays, shorter combustion duration, and lesser diffusion fuel mass.

http://dx.doi.org/10.5772/64470

- Correlation between particle oxidation reactivity and internal nanostructure morphology from the DBE-derived soot by the results of thermogravimetric and transmission electronic microscopic analysis. It is generally found that test fuel with higher oxygen content, larger percentage of volatile organic fractions (VOFs), and lower soot burnout temperature (low activation energy) would have stronger oxidative reactivity with particle morphology of smaller primary particle size and curved, tortuous, and disorganized nanostructures.

2. Experimental investigation

2.1. Test plan

Four sets of experimental investigations were adopted. First, a naturally, water-cooled, four-cylinder direct-injection diesel engine was tested at a steady speed of 1800 rev/min under five engine loads when fueled with diesel-biodiesel containing 15 vol% of waste-cooking-oil biodiesel while the ethanol volume varied from 0 to 20% at a step of 5%. The engine performance and gaseous emission analysis are summarized in Sections 3 and 4, respectively. Second, the correlations between combustion characteristic parameters and the particulate emissions for DBE blends are described in Section 5. Third, the combined effect of DBE blends and intake CO_2 dilution of 1.5–4.5% (at 1.5% interval) is evaluated and tested under a high engine load in Section 6. Finally, the effect of DBE blends on particulate volatility, oxidation properties, and nanostructures is investigated in Sections 7 and 8. The specifications of test engine and test fuels are shown in **Tables 3** and **4**, respectively. The test plan was based on the commonly accepted testing norms [2, 8, 11, 15–20] used in Europe, China, and Hong Kong for comparable results so as to investigate the influence of DBE blends and intake CO_2 dilution under different fuel energy substitutions and engine loads, considering combustion characteristics and emission performance.

Model	**Isuzu 4HF1**
Engine type/combustion chamber shape	Inline four-cylinder DI/Omega
Max. power	88 kW/3200 RPM
Max. torque	285 Nm/1800 RPM
Bore × stroke	112 mm × 110 mm
Displacement	4334/cc or 4.334 l
Compression ratio	19.0:1
Fuel injection timing	8° BTDC
Injection pump type	Bosch inline type
Injection nozzle	Hole type (with five orifices)
Injection nozzle diameter	0.3 mm
Injection nozzle opening pressure	18.1 MPa

Table 3. Specifications of test diesel engine.

Properties	ULSD	Biodiesel	Ethanol	
Cetane number	52	51	6	
Lower heating value (MJ/kg)	42.5	37.5	28.4	
Density (kg/m^3) at 20°C	840	871	786	
Viscosity (mPa S) at 40°C	2.4	4.6	1.2	
Heat of evaporation (kJ/kg)	250–290	300	840	
Carbon content (%mass)	86.6	77.1	52.2	
Hydrogen content (%mass)	13.4	12.1	13	
Oxygen content (%mass)	0	10.8	34.8	
Sulfur content (%mass)	<10	<10	0	
Calculated properties	**DBE0**	**DBE5**	**DBE10**	**DBE20**
Cetane number	51.9	49.6	47.3	42.7
Density (kg/m^3) at 20°C	845	842	839	833
Lower heating value (MJ/kg)	41.7	41.0	40.3	38.9
Oxygen content (%mass)	1.7	3.3	5.0	8.2

Table 4. Properties of blending stocks and test fuels.

2.2. Gaseous and particulate measurement

The schematic and photographs of the experimental system are shown in **Figures 1–3**. The gaseous species including hydrocarbon (HC), nitrogen oxides (NO_x), carbon monoxide (CO), carbon dioxide (CO_2), particulate mass and number concentration (PM and PN) and volatile organic fractions (VOF) were measured. When studying the effect of CO_2 dilution on the engine performance and exhaust emissions using DBE blends, the intake CO_2 concentration was measured at the engine intake manifold. HC was measured with a heated flame ionization detector (HFID); NO_x was measured with a heated chemiluminescence analyzer (HCLA); CO and CO_2 were measured with nondispersive infrared analyzer (NDIR). Exhaust gas temperature was measured with a K-type thermocouple. All gas analyzers were manufactured by California Analytical Instruments, Inc., and calibrated with standard gases and zero span checks before each experiment. A two-stage Dekati minidiluter was used to create a constant volume sampling to obtain a diluted exhaust gas that is representative of the average concentration while engine runs particularly in measuring low-concentration particle mass-number emissions. The primary diluted exhaust gas was delivered to a tapered element oscillating microbalance (TEOM) for measuring particulate mass concentration and then secondary diluted exhaust gas to a scanning mobility particle sizer (SMPS) for measuring the size distribution and number concentration. The dilution ratio (DR) was determined from the measured CO_2 concentrations of background air, undiluted exhaust gas, and diluted exhaust gas. The primary dilution ratio for TEOM was around 11 ± 2 whereas the secondary dilution ratio for SMPS was around 88 ± 7. The exhaust emission measuring instruments are listed in **Table 5**.

http://dx.doi.org/10.5772/64470

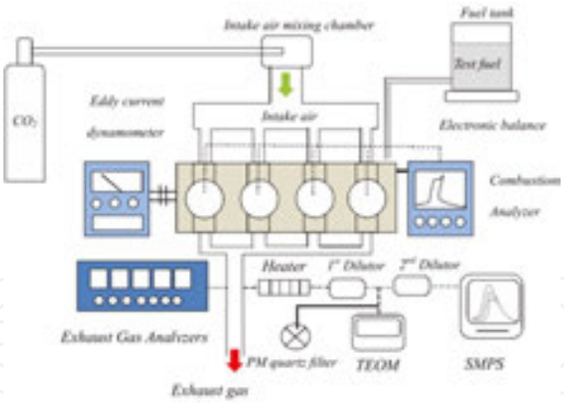

Figure 1. Schematic diagram of the experimental setup.

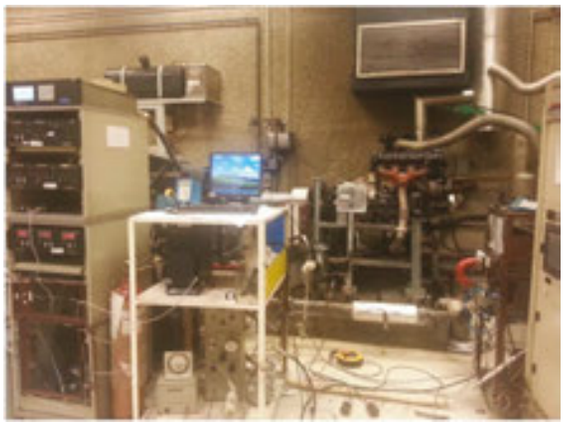

Figure 2. Photograph of the experimental setup.

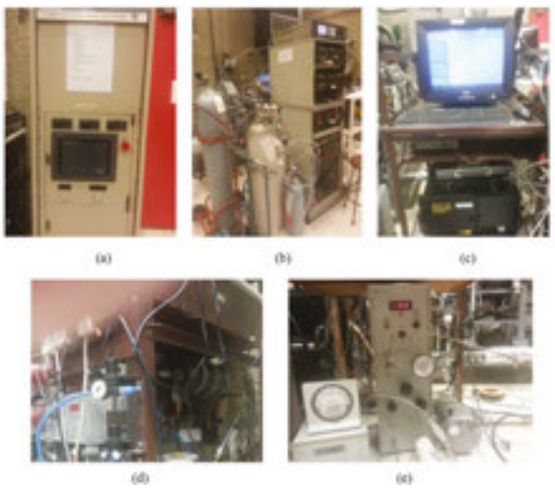

Figure 3. Photographs of (a) engine dynamometer, (b) HFID/HCLA/NDIR gas analyzers, (c) TEOM PM mass analyzer, (d) Dekati minidiluter, and (e) SMPS PM number-size distribution analyzers.

Gas species	Unit	Make/type
HC	ppm	CAI model 300
NO_x/NO	ppm	CAI model 400
CO_2/CO	ppm/%	CAI model 300
PM mass	$\mu g/m^3$	R&P TEOM 1105
PM number and size distribution	$\#/cm^3$	TSI 3934

Table 5. Exhaust emissions measuring instruments.

2.3. Combustion analysis

A Kistler type 6056A piezoelectric pressure transducer was used to measure the in-cylinder pressure at 0.5 crank-angle interval. Crankshaft position was measured by a Kistler crank-angle encoder. The cylinder pressure was averaged over 400 cycles to smooth any combustion cyclic irregularity that may appear in diesel engines fueled with low-ignition-quality biofuels [21] and was then analyzed with a commercial combustion analyzer (DEWETRON, DEWE-ORION-0816-100X) to obtain the heat release rate due to fuel combustion, which is developed under the first law of thermodynamics to obtain the heat released arising from the fuel burned per crank angle.

Figure 4. Photograph of thermogravimetric analyzer.

http://dx.doi.org/10.5772/64470

2.4. Thermogravimetric analysis

Particulate samples used for particulate oxidation property and morphology were collected on the 47 mm quartz filter paper inside a particulate collector with the same diluted condition as TEOM. The transfer line from the exhaust to the dilutor was insulated and heated at around 170°C to avoid volatile HC condensation loss. The investigation of the particulate composition and oxidation property was conducted through the thermogravimetric analysis (TGA) on the particulate sample in an Al_2O_3 crucible. TGA was conducted using the Netzsch STA 449 TGA/DSC (thermogravimetric analysis/differential scanning calorimetry) with a measurement resolution of 25 ng as shown in **Figure 4**. The heating program is listed in **Table 6**. When the TGA temperature was below 400°C, the particulate samples were heated in argon to remove the volatile substance. The samples were then oxidized in air for the investigation of particle oxidation. The total mass loss versus TGA furnace temperature is used to determine the fraction of volatile substances (VS) and nonvolatile substances (non-VS) in the diesel particulate. The volatile substances can be divided into two parts: low- and high-volatility fractions. The volatility fraction versus temperature range is defined below:

Steps	TGA heating program
Devolatilization	
1	Initial atmosphere under argon
2	Isothermal for 10 min
3	Ramp 3°C/min to 45°C
4	Ramp 10°C/min to 400°C
Oxidation	
5	Change atmosphere with air
6	Ramp 10°C/min to 800°C
7	Isothermal for 10 min

Table 6. TGA heating program.

High-volatile substances (H-VS): $50°C \leq T \leq 250°C$, under argon environment

Low-volatile substance (L-VS): $250°C \leq T \leq 400°C$, under argon environment

Nonvolatile substances (non-VS): $400°C \leq T \leq 800°C$, under air environment

2.5. Transmission electronic microscopic analysis

The investigation of particle morphology was conducted through high-resolution transmission electronic microscopy (STEM, JEOL JEM-2100F) as shown in **Figure 5**. The maximum

magnification is up to 910,000× with a measurement resolution of about 0.2 nm. The soot samples were first collected in the 47 mm diameter quartz filter paper and the paper was cut into tiny pieces and mixed with ethanol in cylinder. The particulate sample in the filter paper was extracted ultrasonically in ethanol for 15 min. Droplets of the colloidal solution were dropped on a TEM grid by tweezer and left for drying in atmosphere before arranging image processing. The above procedures shown in **Figure 6** for preparing the TEM samples follow the method suggested by Vander Wal [22].

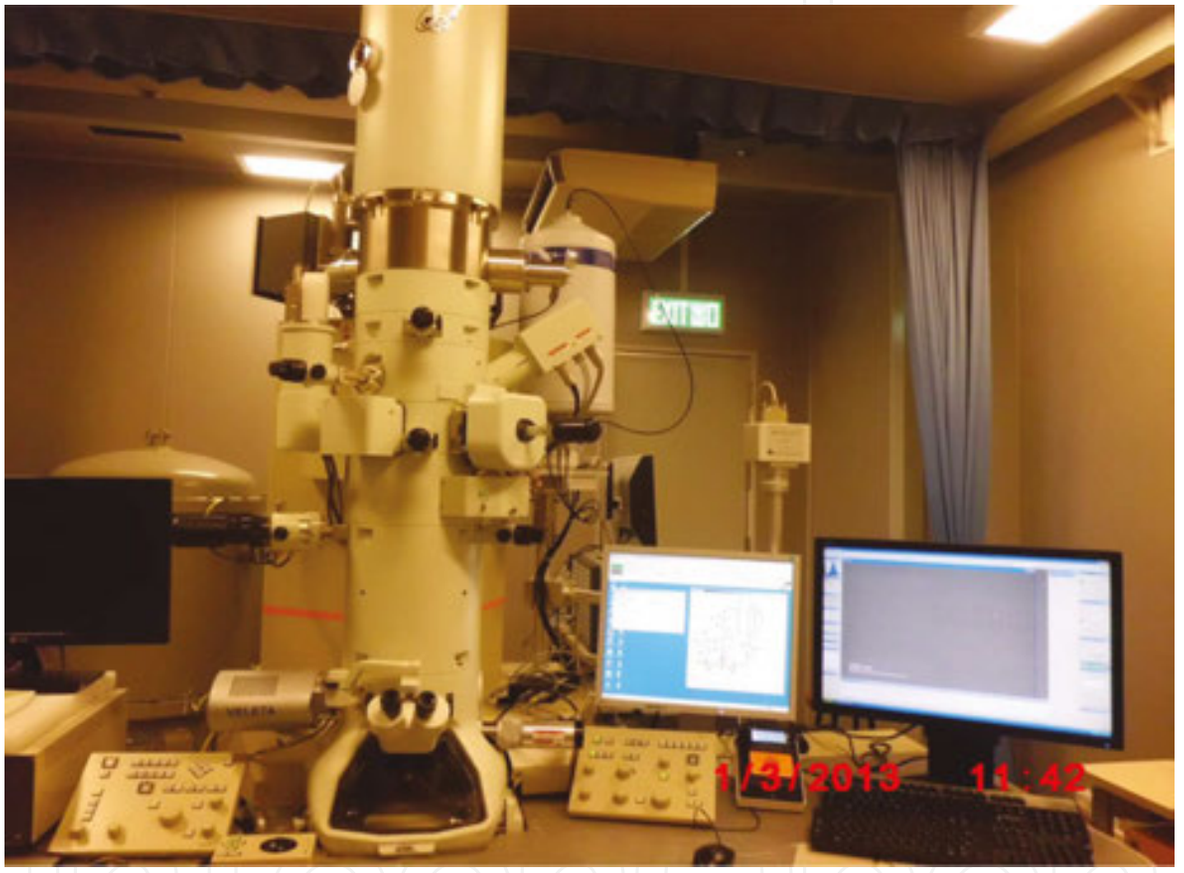

Figure 5. Photograph of high-resolution transmission electronic microscopy.

TEM images were taken from four locations with several aggregates surveyed at the same locations to maintain the consistency of examination. The commercial image processing software Image-Pro Plus 6.0 (Media Cybernetics) was used for analyzing the HRTEM images. From the images, the diameter and width of soot aggregates and primary fine particle with clear boundaries would be measured with the software. The nanostructure of primary fine particles is exhibited in the form of parallel or twisted carbon lamellae. Three parameters including fringe length, fringe separation distance, and tortuosity of the carbon lamellae could be measured and used to describe the nanostructure of particle.

http://dx.doi.org/10.5772/64470

(a) Colloidal solution is ultrasoniced for 15 minutes.

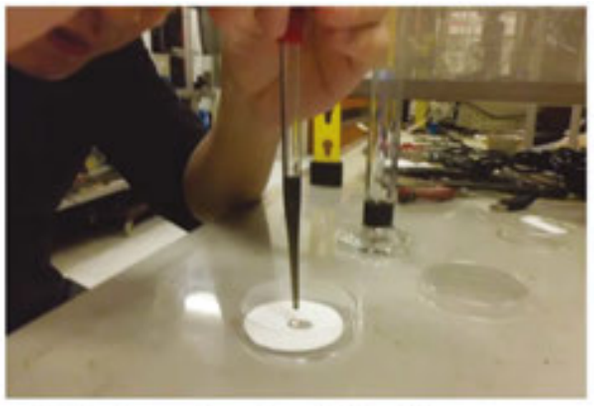

(b) Droplets are dropped on a TEM grid by tweezer.

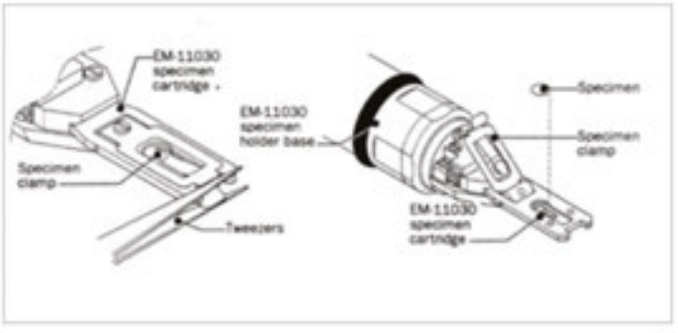

(c) Details of the specimen chamber.

(d) The TEM grid is fixed on the specimen chamber.

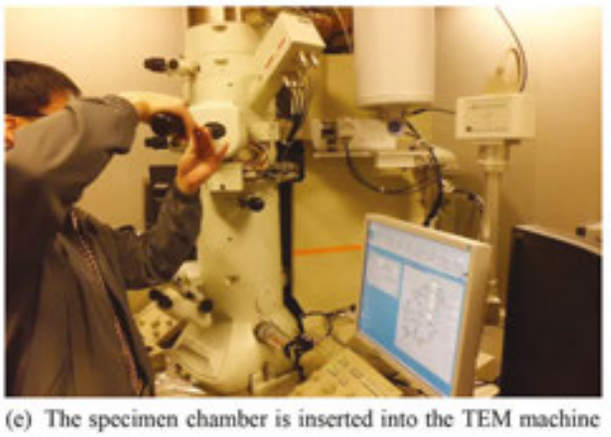

(e) The specimen chamber is inserted into the TEM machine for imaging

Figure 6. Procedures for preparing TEM samples. (a) Colloidal solution is ultrasoniced for 15 min; (b) droplets are dropped on a TEM grid by tweezer; (c) details of the specimen chamber; (d) the TEM grid is fixed on the specimen chamber; (e) the specimen chamber is inserted into the TEM machine for imaging.

2.6. Experimental uncertainties

Successive testing fuels will be filled in both a fuel tank and a 5 l measuring cylinder. There is a manual switch for selecting the fuel source either fed from the fuel tank or the measuring

cylinder to the engine. In order to ensure that the residual fuel from the previous test inside engine is fully consumed, a portion of around 1000 ml successive testing fuel filled in the measuring cylinder would be consumed first by the test engine running for around 5 min at each testing condition after the cooling water reached 80°C and the exhaust gas temperature become stable (±1°C). Upon consuming all the fuels in the measuring cylinder, the fuel source will then switched manually to the fuel tank for formal record of each testing case. The gaseous emissions were converted from volumetric concentrations to brake-specific emissions by employing the SAE J1088 method [23]. The steady-state tests were repeated three times to ensure that the data are repeatable within the experimental uncertainties of the measurements. The experimental uncertainty and standard errors in the measurements have been determined based on the method proposed by Moffat [24]. The measurement results obtained from different fuels were compared with baseline fuel of ultra-low-sulfur diesel (ULSD) using the two-sided Student's *t*-test to testify they are significantly different from each other at the 95% significance level.

3. Engine performance analysis

This section reports the effects of DBE blends on brake-specific fuel consumption, brake thermal efficiency, in-cylinder pressure, heat release rate, combustion duration, and diffusion fuel mass when diesel-biodiesel is blended with different ethanol contents that were tested in a diesel engine at a steady-state speed of 1800 rev/min under five engine loads of 30, 60, 120, 200, and 240 Nm corresponding to the brake mean effective pressure of 0.09, 0.17, 0.35, 0.58, and 0.70 MPa, respectively.

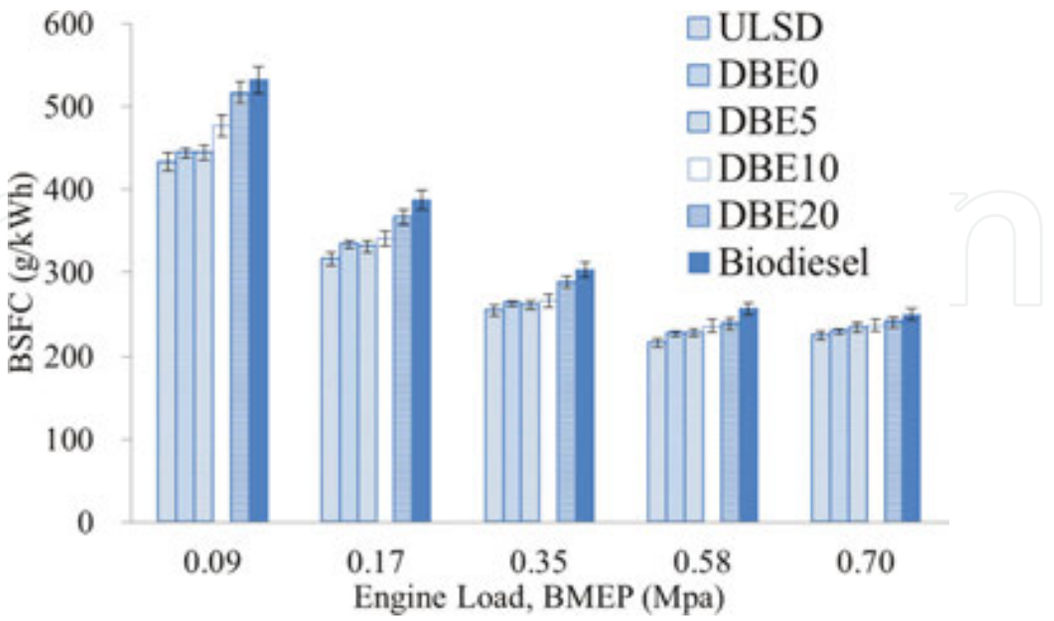

Figure 7. Comparison of BSFC.

http://dx.doi.org/10.5772/64470

3.1. Brake-specific fuel consumption

Figure 7 indicates that the brake-specific fuel consumption (BSFC) of all test fuels decreases with an increase in the engine load from 0.09 to 0.70 MPa with decreasing slope due to an increase in the brake thermal efficiency at higher engine loads. The results are similar to those reported in early works [15, 16, 25]. At each engine load, fuels having lower heating values (LHVs) require a higher fuel mass consumption rate to compensate their low-energy content for generating the same engine power. The maximum LHV (42.5 MJ/kg) belongs to neat diesel, followed by DBE5 (41.04 MJ/kg), DBE10 (40.34 MJ/kg), DBE20 (38.93 MJ/kg), and neat biodiesel (37.5 MJ/kg). At the highest test engine load of 0.70 MPa, the minimum BSFC is 225.3 g/kWh for diesel, followed by 234.8 g/kWh for DBE5, 239.1 g/kWh for DBE10, 240.5 g/kWh for DBE20, and 249.2 g/kWh for neat biodiesel. Therefore, the BSFC for neat biodiesel is the highest due to its lowest energy content while that for diesel is the least among the test fuels. The higher the proportion of ethanol in the DBE blends, the higher the BSFC is.

3.2. Brake thermal efficiency

Figure 8 indicates that the brake thermal efficiency (BTE) increases as a function of oxygen contents in the test fuels and increases with an increase in engine loads. For each engine load, the more the oxygenates are added in the fuels, the lower the heating value of the fuel blends and the higher the BSFC. However, the increase of oxygenates could provide additional lubricity, reduce fuel viscosity, improve atomization, and provide more oxygen contents for improving the combustion process in converting fuel chemical energy into useful engine work. Consequently, BTE is elevated. At the highest test engine load of 0.70 MPa, the maximum BTEs attained for biodiesel, DBE20, DBE10, DBE5, and diesel are 38.53, 37.95, 37.82, 37.36, and 37.10%, respectively. Therefore, there is no obvious variation of BTE among diesel, biodiesel,

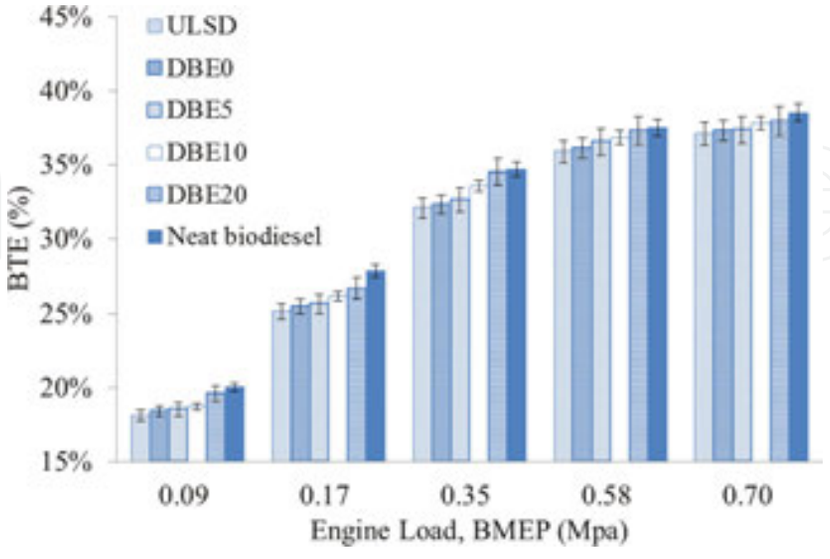

Figure 8. Comparison of BTE.

and the DBE fuels at the high engine load, which is similar to observations reported in the literature [16].

3.3. Cylinder pressure and heat release rate

The variations in the in-cylinder pressure and heat release rate are shown in **Figure 9** for different fuels at the low, medium, and high engine loads of 0.09, 0.35, and 0.70 MPa, respectively. The peak in-cylinder pressure occurs further away from the top dead center (TDC) in the expansion stroke with the increase in the engine load, which is similar to the results of Qi et al. [26]. The peak heat release rate increases with an increase in the engine load from low to the medium, but decreases at the high engine load for all test fuels, which is similar to the results of Zhu et al. [27]. The in-cylinder pressure and the peak heat release rate of DBE blends

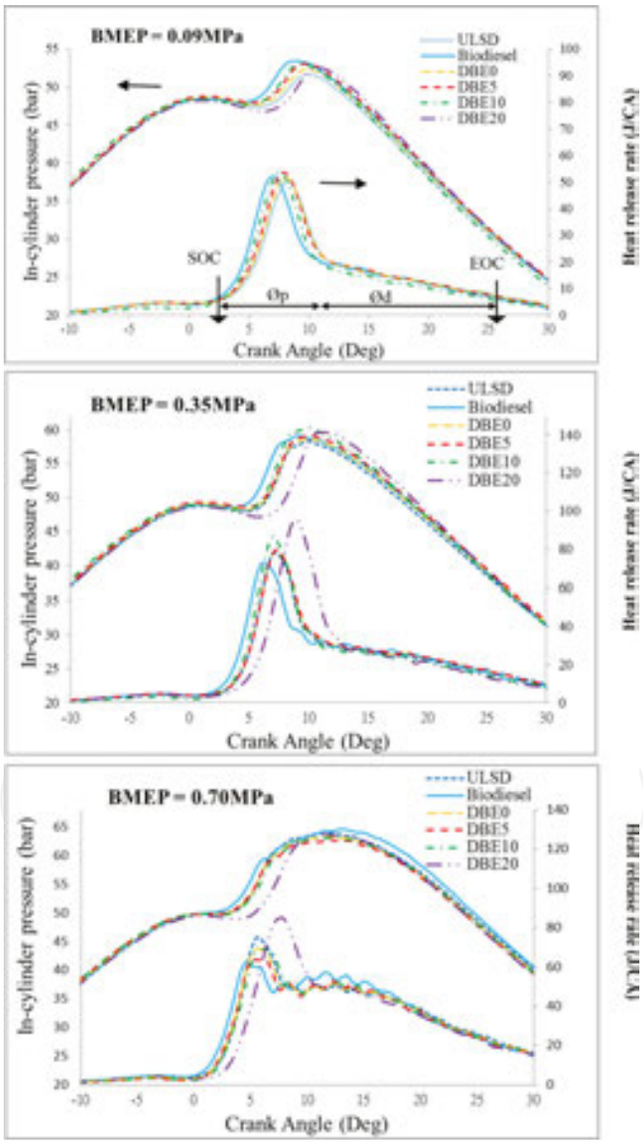

Figure 9. Variation of the in-cylinder pressure and heat release rate.

http://dx.doi.org/10.5772/64470

are comparatively higher than that of ULSD and biodiesel. With the increase of ethanol in the blended fuels, the ignition delay becomes longer. The in-cylinder pressure and peak heat release become higher and retarded due to more fuel burned in the premixed burning phase.

3.4. Start of combustion and combustion duration

The start and duration of combustion for different fuels under different engine loads are shown in **Figure 10**. It can be found that with the increase in the engine load, the start of combustion of all test fuels advances while combustion duration increases. Thus, the ignition delay decreases with the increase in the engine load. For the different fuels, the ignition delay increases in the order of biodiesel, ULSD, DBE0, DBE5, DBE10, and DBE20. The shorter ignition delay of biodiesel compared with ULSD is attributed to its higher bulk modulus of compressibility [28, 29]. Moreover, Sivalakshmi et al. [30] explained that gaseous compounds of low molecular weight, broken down from biodiesel during injection into the engine cylinder at high temperature, could ignite earlier thus reducing the ignition delay and advancing the start of combustion for biodiesel. As for the DBE blends, the increase of ethanol fractions from 0 to 20% increases the ignition delay thereby retarding the start of combustion.

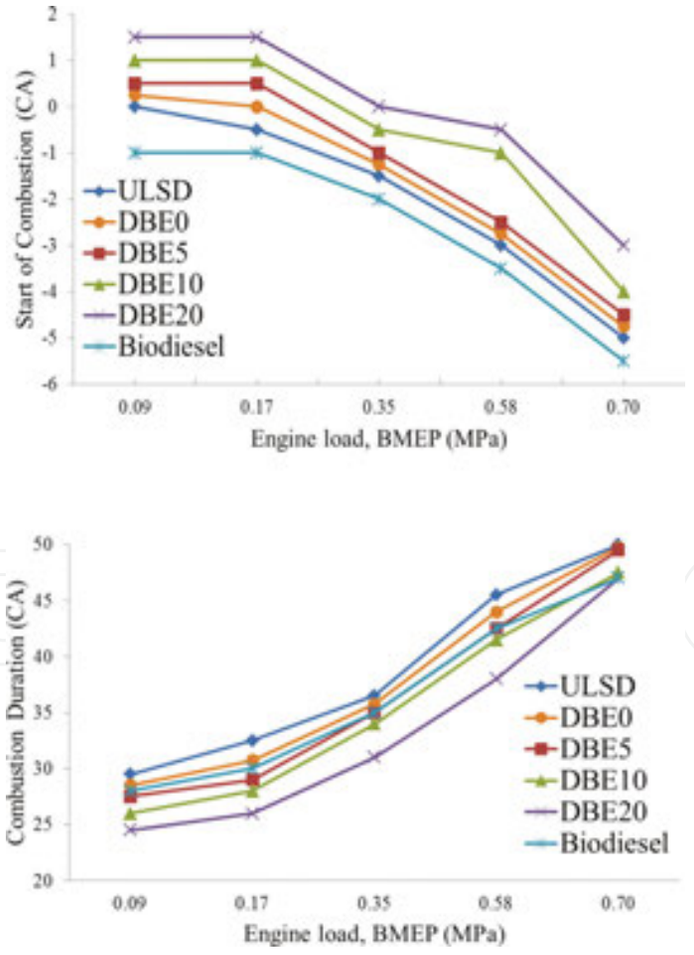

Figure 10. Variation of start of combustion and combustion duration with engine load.

The combustion duration in general increases in the order of DBE20, DBE10, DBE5, biodiesel, DBE0, and diesel. For a specific engine load, the volume of fuel consumed increases in the order of ULSD, DBE0, DBE5, DBE10, DBE20, and biodiesel due to the lower calorific values of biodiesel and ethanol compared with ULSD. DBE blends generally have longer ignition delay, larger amount of fuel burned in premixed mode, and less burned in diffusion mode, resulting in shorter combustion period when compared with biodiesel and diesel fuel for all engine loads. At high engine load, the difference in combustion duration among different fuels decreases as the ignition delay period decreases at a high engine load.

3.5. Total and diffusion fuel mass

Diesel particles are composed of soot, volatile organic fraction, and sulfate, while soot is mainly formed in the diffusion combustion mode. In order to understand the effects of combustion characteristics of different fuels on particulate emission, it is essential to examine their respective mass of fuel burnt in the diffusion mode. The variations of the total fuel mass consumption and diffusion fuel mass consumptions for different fuels with engine load are shown in **Figure 11**.

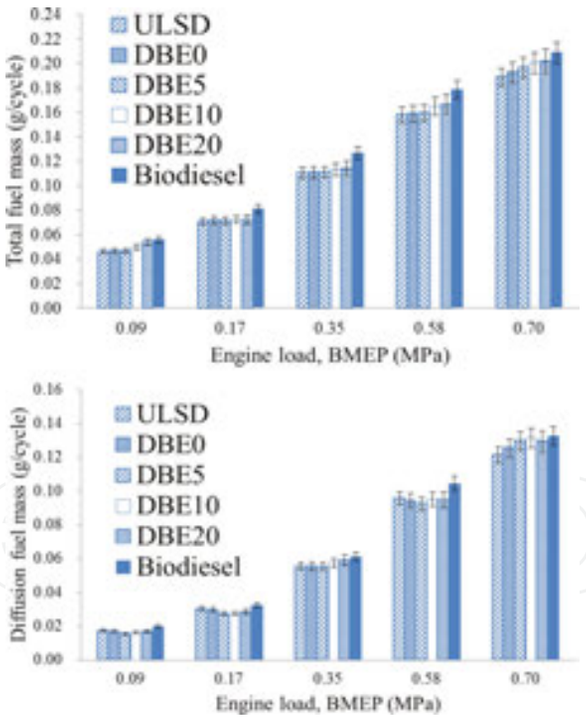

Figure 11. Variation of the total fuel mass and diffusion fuel mass with engine load.

The DBE blends retard the start of combustion and shorten the combustion duration resulting in longer premixed and shorter diffusive combustion duration when compared with biodiesel and ULSD. The higher the ethanol fraction in the blended fuel, the shorter the diffusion combustion duration and the lesser mass of fuel burned in the diffusion mode.

http://dx.doi.org/10.5772/64470

4. Regulated gaseous emission analysis

This section presents the experimental results on exhaust emissions of carbon monoxide (CO), carbon dioxide (CO_2), hydrocarbon (HC), and nitrogen oxides (NO_x) from the test diesel engine at a steady speed of 1800 rev/min under five engine loads when diesel-biodiesel blended with 0, 5, 10, and 20% ethanol. Correlation equations are formulated through a curve-fitting process for predicting percentage changes in CO, CO_2, HC, and NO_x.

4.1. Brake-specific CO and CO_2 emissions

The variations of BSCO and $BSCO_2$ emissions with engine loads are shown in **Figures 12** and **13**, respectively. BSCO decreases with the increase in the engine load. $BSCO_2$ decreases with the increase in the engine load at low engine loads and does not change much with further increase in the engine load from 0.35 to 0.70 MPa. Biodiesel has the lowest BSCO and the highest $BSCO_2$ among all the test fuels in low and medium engine loads, but at similar level with the other fuels at high loads. The BSCO emission increases with the ethanol content in the blended fuel at light and medium engine loads but at similar level at high engine loads. Compared with ULSD, BSCO emissions are increased by 2.97, 2.05, and 37.80% on arithmetic mean under the five different engine loads for DBE5, DBE10, and DBE20, respectively. The $BSCO_2$ emissions generally increase when the ethanol content is increased but the increment becomes less with increasing engine load. Compared with ULSD, $BSCO_2$ emissions are decreased by 4.41, 9.53, and 4.07% on arithmetic mean under the five different engine loads for DBE5, DBE10, and DBE20, respectively, due to a lower carbon-to-hydrogen ratio when increasing the ethanol fractions in fuels.

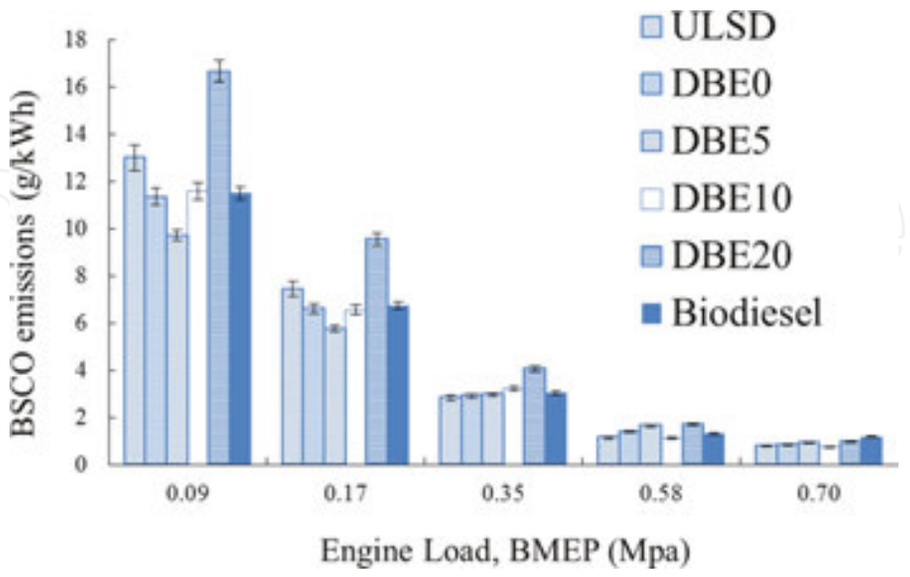

Figure 12. Variation of BSCO with engine loads.

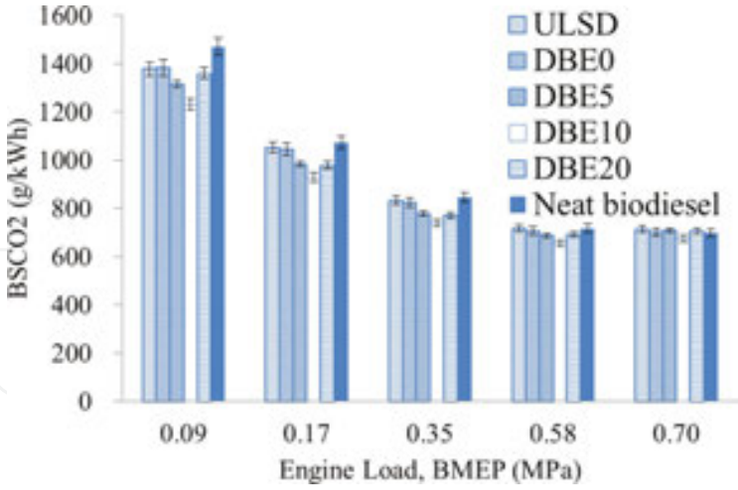

Figure 13. Variation of $BSCO_2$ with engine loads.

4.2. Brake-specific HC emissions

The variation in the brake-specific hydrocarbon (BSHC) emissions with engine load is shown in **Figure 14**. Biodiesel has the lowest BSHC emissions among the test fuels in all engine loads. The BSHC emissions of DBE blends are higher than that of ULSD in all engine loads. BSHC emission decreases with engine load but increases when the ethanol content is increased in the DBE blends at light and medium engine loads but at similar level at high engine loads. Compared with ULSD, BSHC emission decreases with engine load but increases by 45.98, 90.46, and 116.79 on arithmetic mean of the five engine loads for DBE5, DBE10, and DBE20, respectively.

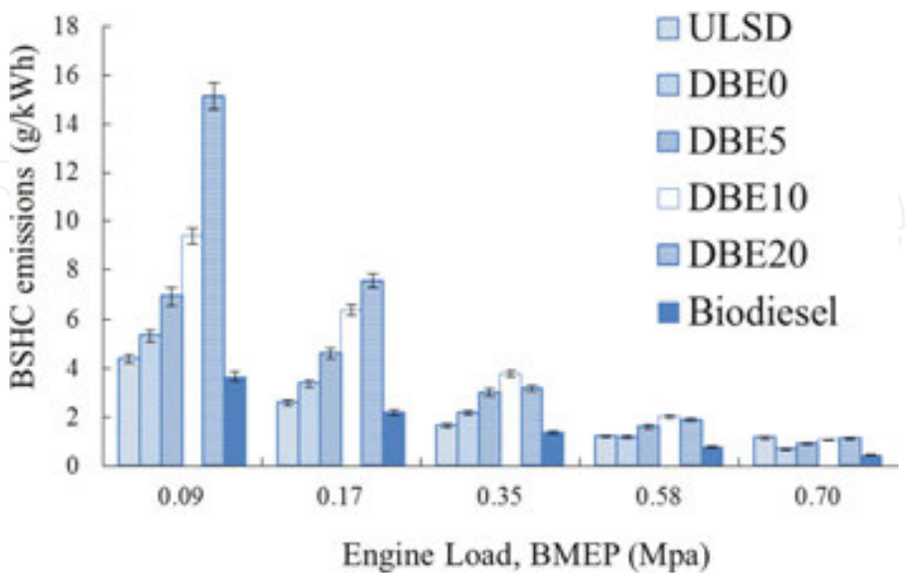

Figure 14. Variation of BSHC with engine loads.

http://dx.doi.org/10.5772/64470

4.3. Brake-specific NO_x emissions

Figure 15 shows the variation of brake-specific NO_x ($BSNO_x$) emissions with engine loads. In general, the $BSNO_x$ decreases with the increase in the engine load. Biodiesel has the highest oxygen content among the test fuels thereby having the maximum temperature during the combustion and thus the highest $BSNO_x$. The lower heating value (LHV) of ethanol is 1.3 times lower than biodiesel and 1.5 times lower than ULSD whereas the latent heat of evaporation of ethanol is about 2.8 times greater than biodiesel and ULSD, which decreases the peak temperature in the cylinder. Thus, the $BSNO_x$ decreases when the ethanol content is increased in the DBE blends from 5 to 20%. In comparison with ULSD, the $BSNO_x$ are reduced by 15–33.3, 2.9–42.4, 4.7–27.5, 4.7–21.5, and 12.5–23.2% corresponding to the five engine loads from 0.09 to 0.70 MPa under different percentages of ethanol in the DBE blends. However, some researchers observed opposite results of DBE blends on NO_x emissions [31]. Probably, in this study, the lower LHV and higher latent heat of evaporation of ethanol are more effective than the lower cetane number and higher oxygen content in influencing NO_x formation.

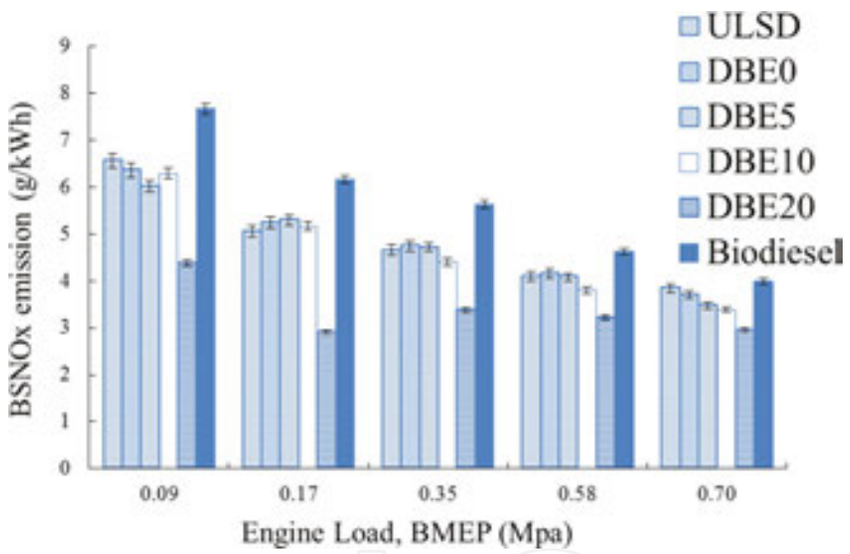

Figure 15. Variation of $BSNO_x$ with engine loads.

4.4. Emission correlation models

Statistical regression correlation is used as a method to determine how diesel engine emissions are affected by the use of DBE blends. The analysis is not intended to predict the absolute regulated emission levels, but rather the percentage change in emissions resulting from the use of DBE. The correlations are obtained by modifying the models proposed by USEPA for diesel-biodiesel blended fuels [8]. Based on the experimental data, the numerical values of the coefficients for the emission correlations obtained through statistical curve fitting are shown in **Table 7**. While for test of significance for the combination of vol% of biodiesel and ethanol, the results are shown in **Table 8**. It can be noted that the combined use of biodiesel and ethanol in DBE blends shows a significant effect in reducing the brake-specific NO_x and PM emissions

simultaneously. However, the increase of ethanol in DBE blends can increase the brake-specific CO and HC emissions due to its cooling effect on the in-cylinder gas temperature. In general, the DBE blends can reduce the above pollutants in particularly with more significant effects in reducing brake-specific CO, HC, and PM emissions. The correlation models provide engine makers or operators a tool to evaluate emissions on the use of DBE blends:

$$\%\ \text{change in BSNO}_x\ \text{emission} = (e^{[-0.0145(\text{vol\% biodiesel})]}e^{[-0.0250(\text{vol\% ethanol})]} - 1) \times 100\% \quad (1)$$

$$\%\ \text{change in BSCO emission} = (e^{[-0.0010(\text{vol\% biodiesel})]}e^{[-0.0331(\text{vol\% ethanol})]} - 1) \times 100\% \quad (2)$$

$$\%\ \text{change in BSHC emission} = (e^{[-0.0293(\text{vol\% biodiesel})]}e^{[-0.0030(\text{vol\% ethanol})]} - 1) \times 100\% \quad (3)$$

Brake-specific emission	Coefficient "a" for vol% biodiesel	Coefficient "b" for vol% ethanol
NO_x	−0.0145	−0.0250
CO	−0.0010	0.0331
HC	−0.0293	0.0030

Table 7. Coefficients for basic emission correlations.

Emission	NO_x	CO	HC
Mean square	0.0538	0.3926	1.271
Adjusted R^2	0.9796	0.9759	0.9897
Standard error	0.0271	0.0419	0.0490
F value	73.0558	223.6300	528.7205
Significance	0.0824	2.1264E−08	4.6598E−10

Table 8. Test for significance of combination of vol% biodiesel and vol% ethanol.

5. Particulate mass-number emission analysis

This section presents the experimental results on exhaust emissions of brake-specific PM emissions, combustion characteristics on PM, particle size distribution, particle number concentrations, and tradeoff relations among PM, PN, and NO_x from the test fuels.

http://dx.doi.org/10.5772/64470

5.1. Particle mass emission

Figure 16 shows that the brake-specific particulate mass (BSPM) emission of each tested fuel decreases with engine load from 0.09 to 0.35 MPa while increases from 0.58 to 0.70 MPa. At low engine loads, the fuel is burned mainly in the premixed mode and more time is available for soot oxidation, resulting in lower particulate formation. When engine load is increased, more fuel is injected into the combustion chamber and hence more fuel is burnt in the diffusion mode while less time is available for soot oxidation, leading to higher particulate formation at high engine load [16]. However, the brake thermal efficiency increases with engine load, leading to the lowest BSPM emission at the engine load of 0.35 MPa.

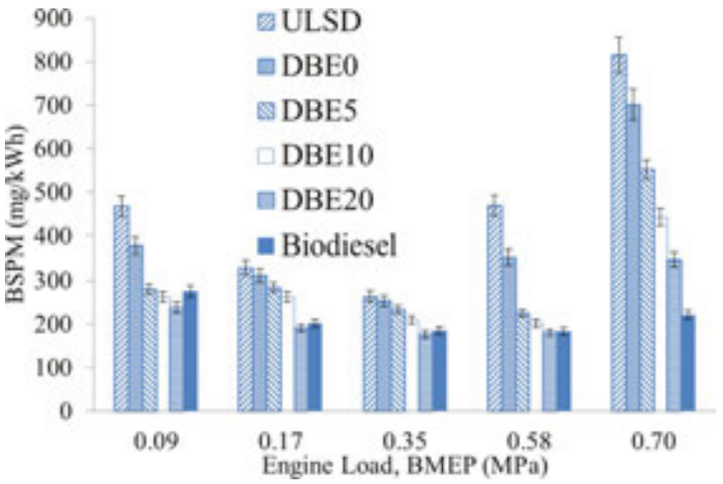

Figure 16. Variation of BSPM with engine loads.

ULSD, which has no oxygen in the fuel, has the highest BSPM among the tested fuels at all loads. When compared with ULSD, the DBE blends could effectively reduce BSPM by 19–49% at 0.09 MPa, 5–42% at 0.17 MPa, 4–33% at 0.35 MPa, 25–61% at 0.58 MPa, and 14–57% at 0.70 MPa for ethanol fractions of 0–20%. The percentage reduction increases with increase of ethanol fractions in the blended fuels. Biodiesel has the highest oxygen contents in the fuel and BSPM is always lower than that of ULSD and DBE0, but its BSPM is close to that of DBE5 at 0.09 MPa, close to that of DBE20 at 0.17–0.58 MPa, and is the lowest among all fuels at 0.79 MPa. The reduction of BSPM is resulted from the reduction of soot and sulfate in particulate. The DBE blends have oxygen concentration ranging from 1.7 to 8.2%. They are also effective in reducing BSPM emissions, compared with ULSD, due to the increasing displacement of diesel fuel by ethanol which has higher oxygen content and lower fuel aromatics and fuel sulfur, all of which are favorable for reducing soot formation.

5.2. Particle number emission

Influence of particles to the environment and human health depends not only on their mass concentration, but also on their number concentration and size distribution. It has been hypothesized that particle toxicity increases with decreasing size due to the higher specific

surface area of smaller particles [32]. It is generally believed that nanoparticles are more dangerous and hazardous to health. Therefore, the particles investigated by SMPS in this study are classified into three groups: (i) total number of particles, (ii) ultrafine particles with diameter less than 100 nm, and (iii) nanoparticles with diameter less than 50 nm. The results, including brake-specific particle number concentration (BSPN) and percentages of both ultrafine and nanoparticles evaluated based on the total particle numbers, are shown in **Table 9**.

1800 rev/min	Parameters	ULSD		Biodiesel		DBE0		DBE5		DBE10		DBE20	
0.09 MPa	BSPN (#/kWh)	1.61E+15		1.96E+15		8.07E+14		1.62E+13		1.38E+13		9.84E+12	
	Total number (#/cm^3)	3.05E+07		3.48E+07		1.54E+07		3.22E+05		2.65E+05		2.59E+05	
	Ultrafine particle (#/cm^3)	2.74E+07	89.8%	3.35E+07	96.3%	1.35E+07	90.3%	3.02E+05	93.7%	2.51E+05	94.7%	2.46E+05	95.3%
	Nanoparticle (#/cm^3)	1.54E+07	50.5%	2.33E+07	67.0%	7.48E+06	55.2%	1.90E+05	59.0%	1.65E+05	62.3%	1.69E+05	65.2%
0.35 MPa	BSPN (#/kWh)	9.21E+14		9.96E+14		4.64E+14		8.86E+12		7.90E+12		6.46E+12	
	Total number (#/cm^3)	5.15E+07		5.40E+07		2.60E+07		5.18E+05		4.67E+05		3.77E+05	
	Ultrafine particle (#/cm^3)	4.39E+07	85.3%	4.97E+07	92.0%	1.96E+07	75.5%	4.09E+05	78.9%	4.16E+05	89.1%	3.43E+05	90.9%
	Nanoparticle (#/cm^3)	2.17E+07	42.1%	2.90E+07	53.7%	8.87E+06	45.2%	2.52E+05	48.6%	2.27E+05	48.6%	1.95E+05	51.7%
0.70 MPa	BSPN (#/kWh)	1.53E+15		1.49E+15		7.88E+14		1.27E+13		1.22E+13		1.33E+13	
	Total number (#/cm^3)	1.25E+08		1.27E+08		6.30E+07		1.05E+06		1.03E+06		1.16E+06	
	Ultrafine particle (#/cm^3)	7.99E+07	63.9%	1.16E+08	91.2%	4.36E+07	69.2%	7.39E+05	70.3%	7.47E+05	72.5%	8.46E+05	72.9%
	Nanoparticle (#/cm^3)	2.74E+07	21.9%	6.84E+07	53.8%	1.24E+07	28.5%	3.82E+05	36.3%	4.58E+05	44.5%	5.85E+05	50.4%

Table 9. Particulate emissions for different test fuels.

For each fuel, the total particle numbers, ultrafine particles, and nanoparticles increase with engine load, while BSPN is the highest at 0.09 MPa and lowest at 0.35 MPa. The increase in the aforesaid three number concentration is associated with the increasing amount of fuel with engine load and hence carbon mass with engine load. Labecki et al. [33] reported that the number concentration of nuclei mode particles (i.e., particle size < 100 nm) increased as the

http://dx.doi.org/10.5772/64470

fuel injection pressure increased at higher engine load while the number concentration of accumulation mode (i.e., 100 nm < particle size < 2500 nm) decreased with an increase in the injection pressure.

At each engine load, biodiesel is generally observed to achieve the highest in BSPN, total number, ultrafine, and nanoparticle emissions among the tested fuels although it has the lowest BSPM in most cases. Various reasons have been provided in the literature for increased particulate number concentration associated with biodiesel. Some researchers explained that biodiesel reduced soot emission due to the reduced soot surface growth rate weakening the ability of condensation and adsorption of volatile organic fractions on soot particle such that high supersaturation may lead to form more nuclei mode particles [34–36]. Tsolakis [37] reported that the higher production of smaller particles from biodiesel was due to its higher viscosity thereby increasing the fuel injection pressure for better fuel atomization and air fuel mixing. Pang [38] also found that the increased fuel injection pressure could affect particle size distribution and increase the number of nuclei mode particles during his study with a heavy-duty diesel engine.

DBE blends with ethanol could reduce BSPN, total particle numbers, ultrafine particles, and nanoparticles by 99% on average for all engine loads as compared with both biodiesel and ULSD. It is due to the combined effects of the presence of fuel-bound oxygen, reduced aromatics and sulfur compound, and the alcohol structure in ethanol which are effective on reduction of soot precursors than methyl-ester structure [39] and the subsequent reduction in particle numbers. Di et al. [17] also reported that diesel-ethanol blends gave lower total number concentrations, ultrafine particles, and nanoparticles than ULSD while diesel-biodiesel blends showed the opposite trends. Thus, besides the particulate mass reduction, DBE also plays an important role in particle number reduction.

For each fuel, the percentages of both ultrafine and nanoparticles in the total particle numbers decrease with increasing engine load, implying that the emitted particles become larger in size. Biodiesel has the highest percentage of ultrafine and nanoparticles because of its higher fuel viscosity that favors higher production of smaller particles. ULSD has the lowest percentage of ultrafine and nanoparticles, implying that larger particles are emitted than biodiesel and DBE blends.

5.3. Tradeoff relations among PM, PN, and NO_x

There is tradeoff between PM and NO_x emissions due to their contradictory responses to oxygen content in fuel. It is well known that biodiesel could reduce PM emissions but lead to an increase in NO_x emissions. Adding ethanol to a diesel fuel could reduce NO_x emissions because of the cooling effect associated with the high latent heat of evaporation of ethanol. **Figures 17** and **18** show that increasing ethanol from 0 to 20% in the DBE blends gives lower BSPM, BSPN, and $BSNO_x$ simultaneously than ULSD, weakening the PM-PN-NO_x tradeoff relationship, while compared with biodiesel, DBE blends give lower $BSNO_x$ and BSPN but higher BSPM.

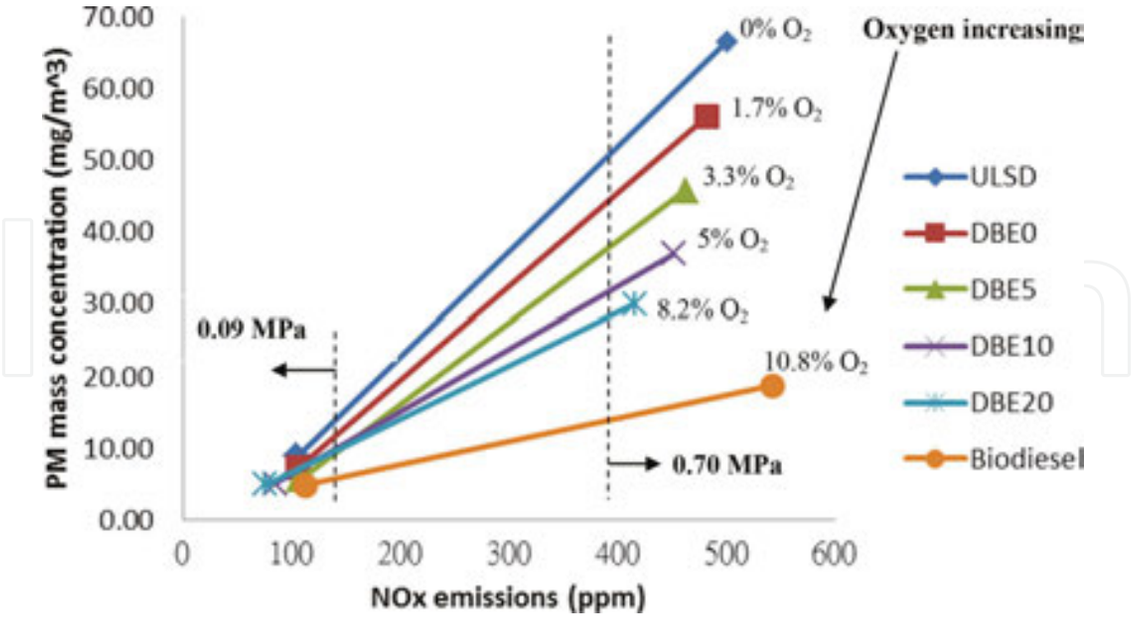

Figure 17. PM-NO_x tradeoff curves for different fuels at loads of 0.09 and 0.70 MPa.

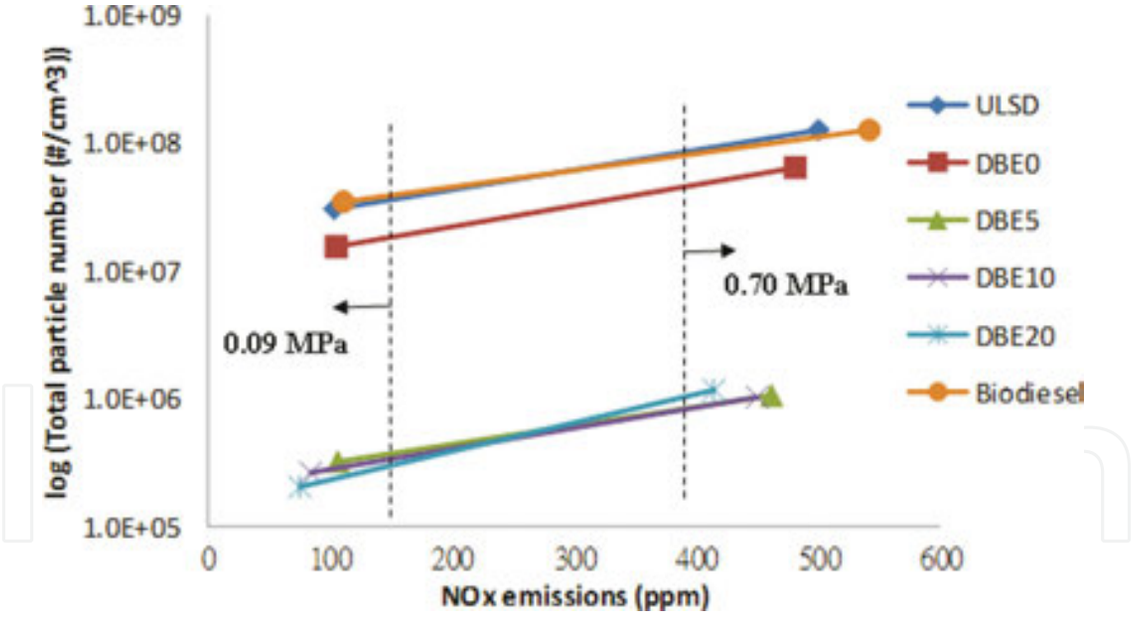

Figure 18. PN-NO_x tradeoff curves for different fuels at loads of 0.09 and 0.70 MPa.

6. Intake charge dilution

This chapter presents the experimental studies on using CO_2 to dilute the intake air of the test diesel engine to reduce NO_x while minimizing the adverse impact on particulate emissions.

http://dx.doi.org/10.5772/64470

The evaluations cover the brake-specific fuel consumption, brake thermal efficiency, combustion characteristics, brake-specific NO_x, brake-specific PM mass, and particle number emissions for diesel-biodiesel blended with 5, 10, and 20% ethanol with intake CO_2 of 1.5, 3, and 4.5% tested at a steady speed of 1800 rev/min under a high engine load of 0.58 MPa.

6.1. Brake-specific fuel consumption and thermal efficiency

At the engine load of 0.58 MPa with no intake dilution, the brake-specific fuel consumption, from the lowest to the highest, is 216.5 g/kWh for ULSD, 237.5 g/kWh for DBE5, 238.2 g/kWh for DBE10, 241.5 g/kWh for DBE20, and 255.9 g/kWh for biodiesel. The brake thermal efficiency attained for ULSD, DBE5, DBE10, DBE20, and biodiesel is 35.9, 34.2, 34.1, 33.6, and 31.6%, respectively. Increasing the ethanol fractions in DBE blends will increase the BSFC and reduce the BTE. **Figure 19** shows the effect of intake CO_2 concentration on BSFC and BTE of DBE blends at the engine load of 0.58 MPa. Increasing the intake CO_2 dilution ratio from 1.5 to 4.5% resulted in a drop in BSFCs by 0.82–1.89% for DBE5, 1.06–1.99% for DBE10, and 0.85–1.52% for DBE20, correspondingly there is an increase in BTE of 0.86–2.01% for DBE5, 1.12–2.12% for DBE10, and 0.89–2.64% for DBE20. In this particular case, CO_2 dilution leads to longer delay, resulting in higher peak pressure, higher peak heat release rate, and hence a slight improvement in BSFC and BTE.

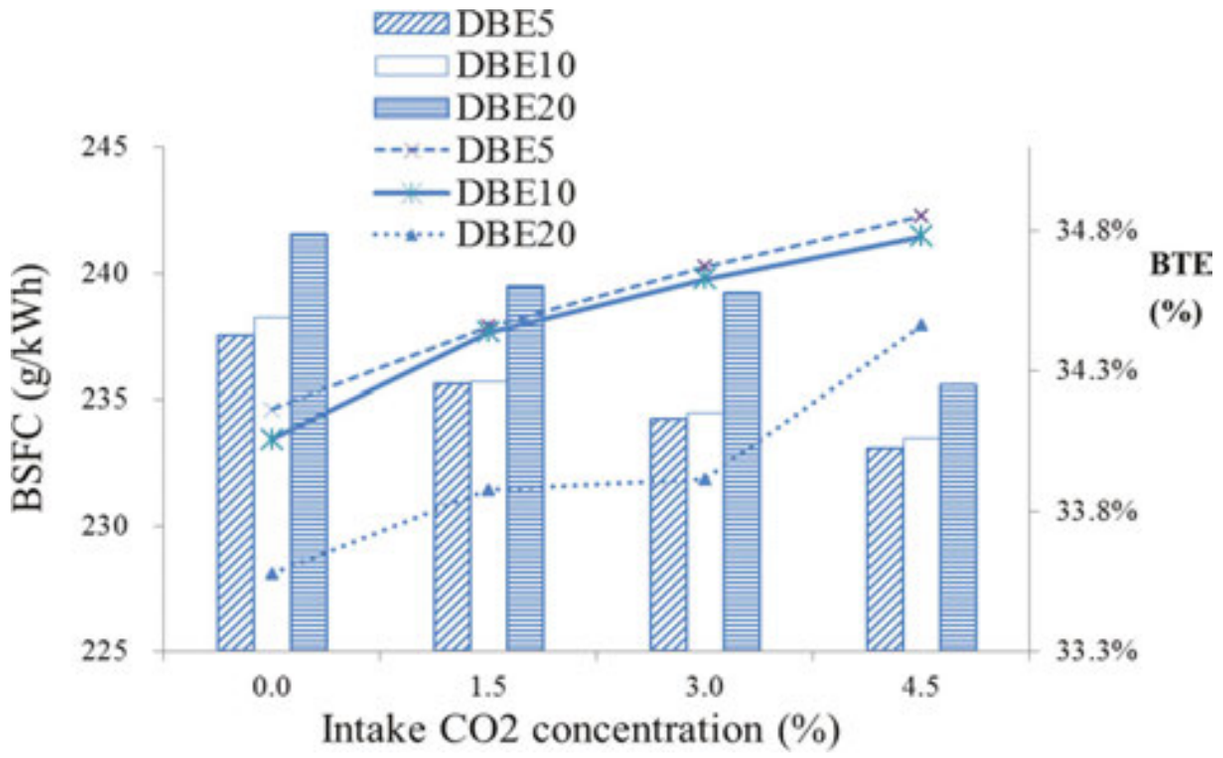

Figure 19. Effect of intake CO_2 on BSFC and BTE of DBE blends at load of 0.58 MPa.

6.2. Combustion characteristics

At the engine load of 0.58 MPa, the exhaust gas temperature of DBE5, DBE10, and DBE20 decreased from 477–467, 471–461, and 481–464°C, respectively, when CO_2 dilution was changed from 0 to 4.5%, indicating less loss in the engine exhaust. The combustion temperature reduced when CO_2 was added due to the higher specific heats of CO_2 than air. Increasing ethanol fractions in DBE blends gives higher and later peak combustion pressure and heat release rate [40]. **Figure 20** shows the in-cylinder pressure and heat release rate (averaged over 400 cycles) of DBE20 at different percentage of CO_2 dilution. Similar results are obtained for DBE5 and DBE10. In general, when intake CO_2 is applied, the maximum in-cylinder pressure increased and occurs further away from the top dead center in the expansion stroke while the peak heat release rate increased and occurs later. Increasing the CO_2 ratio from 0 to 4.5% has attained peak heat release rate of 70.7–113.3 J/°CA for DBE5, 100.1–116.8 J/°CA for DBE10, and 110.0–124.5 J/°CA for DBE20. The peak in-cylinder pressure attained for DBE5 is from 61.8 to 67.9 bar, for DBE10 is from 63.8 to 68.4 bar, and for DBE20 is from 67.6 to 68.9 bar. The in-cylinder pressure and heat release rate increased with more intake CO_2 due to the changes in thermodynamic properties of intake mixture. When intake CO_2 is applied, the ignition delay of DBE blends is further enhanced due to the reduction of oxygen and increase of specific heats of the intake charge. Therefore, a larger amount of fuel is injected into the cylinder and more fuel is prepared for combustion during the ignition delay period. When combustion starts, a greater amount of fuel is quickly consumed thereby increasing the in-cylinder pressure and heat release rate.

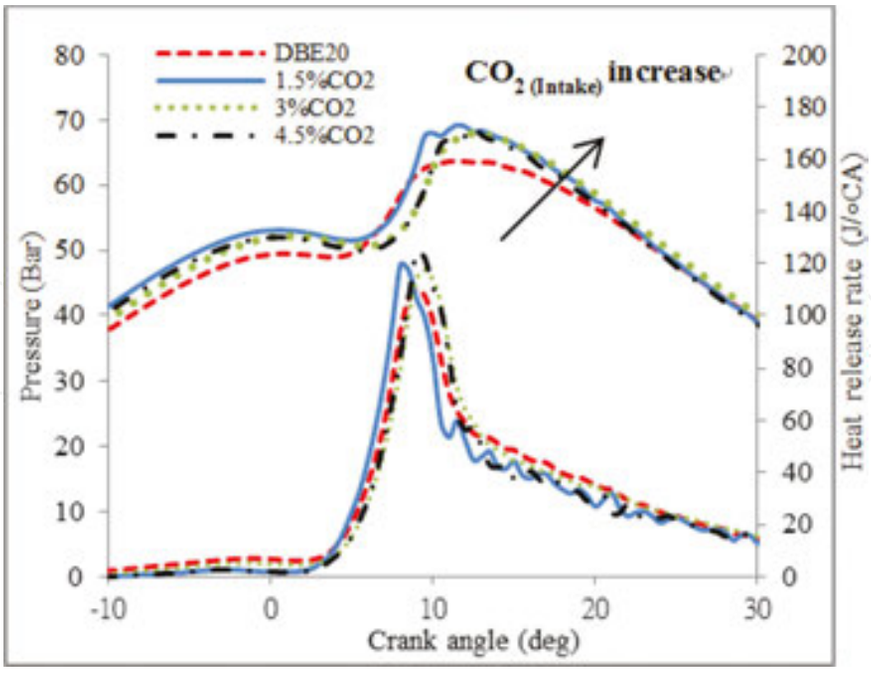

Figure 20. Effect of intake CO_2 on in-cylinder pressure and HRR of DBE20 at the engine load of 0.58 MPa.

http://dx.doi.org/10.5772/64470

6.3. Brake-specific NO_x emission

At the engine load of 0.58 MPa with no CO_2 dilution, the $BSNO_x$ is 4.75 g/kWh for biodiesel, 4.52 g/kWh for ULSD, 4.47 g/kWh for DBE5, 4.43 g/kWh for DBE10, and 3.64 g/kWh for DBE20. DBE blends could reduce NO_x emission compared with ULSD and biodiesel. When introducing CO_2 in the intake from 1.5 to 4.5% to DBE blends, the $BSNO_x$ are further reduced, leading to reductions of 9.2–70.6, 23.7–73.1, and 31.5–76.7% for DBE5, DBE10, and DBE20 respectively, as compared with ULSD as shown in **Figure 21**. There are several factors leading to the enhancement of NO_x reduction in DBE blends by CO_2 dilution. The addition of CO_2 significantly reduces the molecular oxygen and nitrogen in intake air reducing the engine-out NO_x emission. The high specific heat of CO_2 would help lowering the combustion temperature thereby suppressing the formation of NO_x from DBE blends.

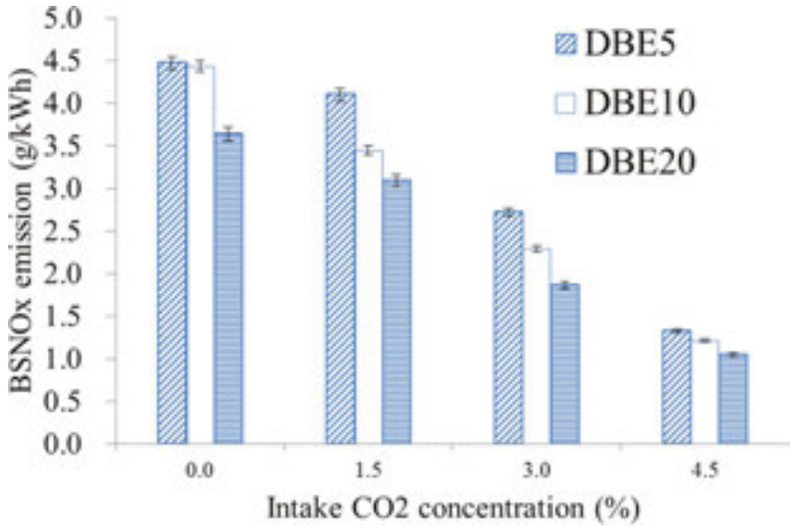

Figure 21. Effect of intake CO_2 on $BSNO_x$ of DBE blends at the engine load of 0.58 MPa.

6.4. Brake-specific PM emission

At the engine load of 0.58 MPa with no intake dilution, the maximum brake-specific particulate mass emissions (BSPM) is 469 mg/kWh for ULSD, followed by 273 mg/kWh for DBE5, 227 mg/kWh for DBE10, 207 mg/kWh for DBE20, and 184 mg/kWh for biodiesel. Increasing the ethanol fractions in DBE blends lowers the BSPM. DBE blends in general perform better than ULSD for BSPM reduction by 49.76% on average while biodiesel has attained the least BSPM emissions among the test fuels. When introducing intake CO_2 from 1.5 to 4.5%, BSPMs for the blended fuels increased but are still lower than that of ULSD but with BSPM reduction dropping from 49.76 to 36.62% on average for the three DBE blends. For individual DBE blends, the BSPM increased by 6.3–40.5% for DBE5, 2.1–29.8% for DBE10 and 0.4–47.2% for DBE20 with intake CO_2 of 1.5–4.5%. The dilution effect from CO_2 is dominant for reducing oxygen in combustion thereby increasing particulate emissions. This is because when intake air is replaced with CO_2, oxygen concentration is reduced. Besides, CO_2 would absorb some of the

released heat. Less heat will then be released during combustion to oxidize the carbon molecules [18]. With increasing CO_2 concentration, such dilution effect is greater than the chemical effect resulted from the dissociation reaction of CO_2 to nullify its soot suppression. Ladommatos et al. [41] reported that the chemical effect from CO_2 to form free radicals for soot suppression was only moderate.

6.5. Brake-specific PN emission

The use of DBE blends, compared with ULSD and biodiesel, could produce less total number of particle concentration of all sizes from low to high engine loads [40]. Increasing the ethanol fractions from DBE5 to DBE10, the carbon content of the blended fuel decreased and oxygen content increased leading to reduction of nuclei particles and total number concentration as shown in **Table 9**. **Figure 22** shows that when adding 1.5% intake CO_2 to DBE blends, there is a decrease in the brake-specific particle number concentration (BSPN). The BSPN however increased with increase of intake CO_2. This effect can also be observed from **Figure 23** which shows the size distributions for DBE20 against CO_2 intake at the engine load of 0.58 MPa. The initial decrease in BSPN with 1.5% CO_2 intake may be a consequence of the dissociation of intake CO_2 which has moderate effects on soot suppression. However, when CO_2 intake increases from 1.5 to 4.5% in the blended fuels, the size distribution curves move upward indicating an increase in the particle number concentration with larger diameter particles. The BSPNs at 4.5% CO_2 intake are higher than those obtained without CO_2 dilution. This is because the dilution effect of CO_2 becomes dominant nullifying the effect of CO_2 dissociation [41]. The reduction of oxygen concentration from the dilution effect therefore increases the particulate mass and particle number concentrations.

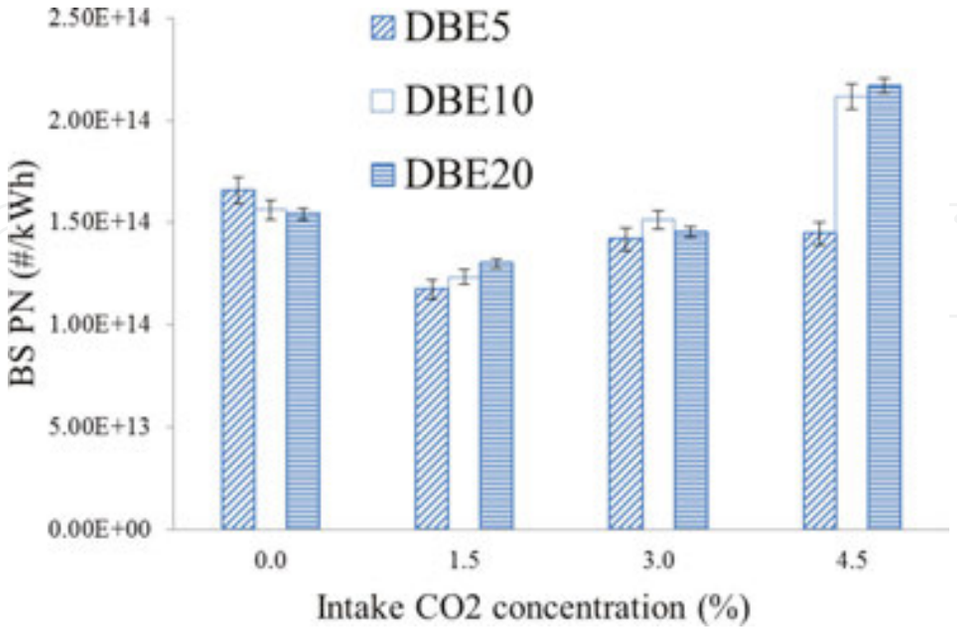

Figure 22. Effect of intake CO_2 on BSPN of DBE blends at the engine load of 0.58 MPa.

http://dx.doi.org/10.5772/64470

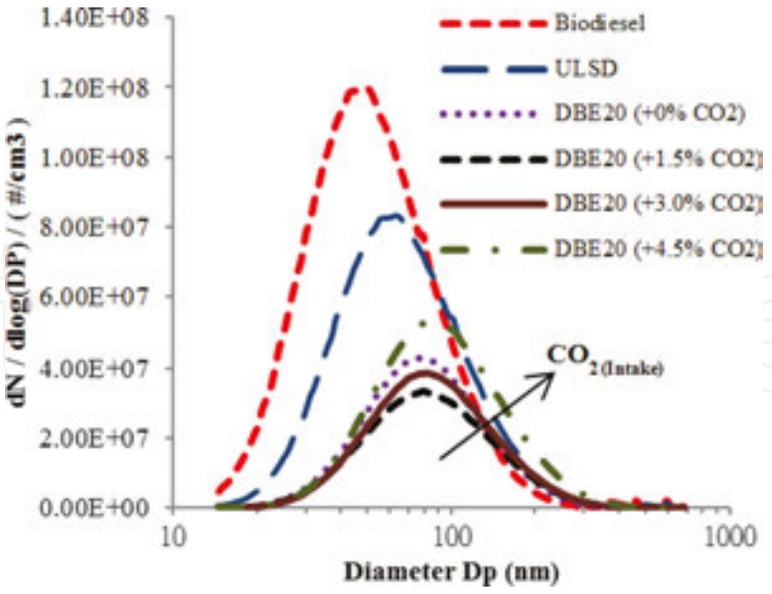

Figure 23. Effect of intake CO_2 on size distribution of DBE20 at the engine load of 0.58 MPa.

7. Thermogravimetric analysis

This section presents the experimental TGA analysis to compare the particle volatility and oxidative reactivity from DBE-derived soot under different blending compositions with those from ULSD and neat biodiesel. The reactivity of particulate samples can be related to the differences in fuel oxygen contents, percentage of VOCs, and soot burnout temperature. Hence, the evaluations would cover brake-specific VOF emissions, soot ignition temperature, activation energy, and oxidative reactivity for DBE blends tested at a steady speed of 1800 rev/min under a high engine load of 0.58 MPa.

7.1. Particle volatility

Figure 24 shows particulate mass reduction curves for different fuels at the engine load of 0.58 MPa. For each fuel, obvious carbon mass losses were found at two different temperature segments: (i) below 300°C and (ii) 550–700°C, representing loss of the volatile organic fraction and oxidation of the nonvolatile fraction, respectively. **Figure 25** shows the effect of fuel type and engine load on the volatile organic fractions (%VOF) in PM emissions. It can be seen that no matter what kind of fuel is used, %VOF decreases remarkably from 27.8 to 11.2% for ULSD, 36.6 to 14.6% for DBE0, 41.5 to 15.0% for DBE5, 46.0 to 17.7 % for DBE10, 48.7 to 19.5% for DBE20, and 73.8 to 29.5% for biodiesel with an increase in the engine load from 0.17 to 0.58 MPa. It is because VOF consisting of unburned HC is removed significantly under high combustion temperature at high load. For different fuels under each engine load, %VOF is affected and increased with increasing oxygen contents in the fuels, being the lowest for ULSD; increasing with ethanol additions in the blended fuels; and up to the highest for biodiesel, as shown in **Figure 25**. The higher %VOF in soot particles originating from oxygenated fuels like

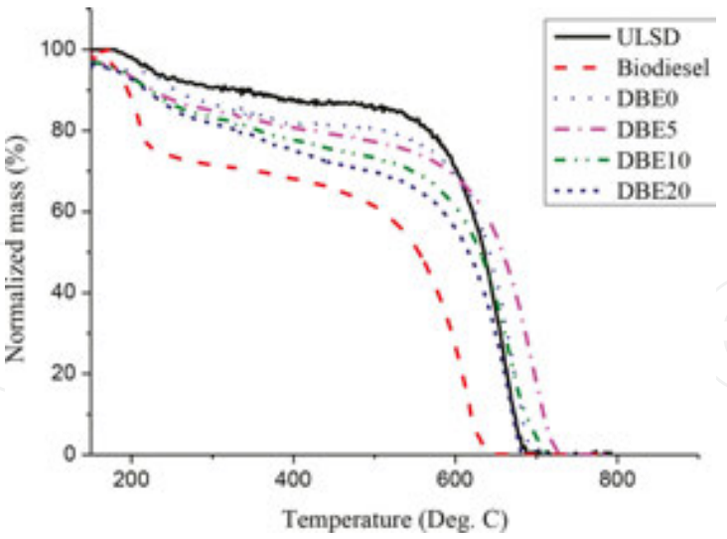

Figure 24. Particulate mass reduction curve for different fuels at a high engine load of 0.58 MPa.

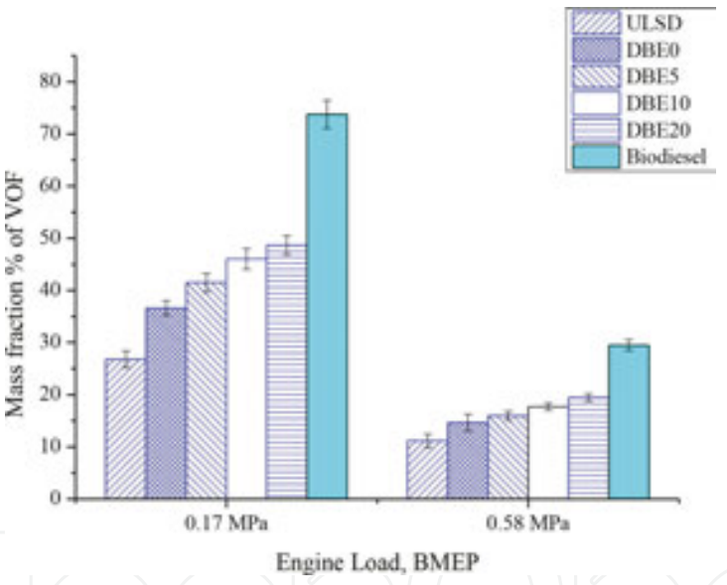

Figure 25. Mass fraction % of VOF with different fuels at two different engine loads.

biodiesel is associated with the higher surface/volume ratio of these particles, implying more pores for condensation and adsorption of unburned HC. **Figure 26** shows the brake-specific VOF emission (BSVOF). At 0.17 MPa, comparing the different fuels, the BSVOF increases with increasing oxygen content in the fuel despite there is a decrease in BSPM with increasing oxygen content in the fuel. However, at 0.58 MPa, it decreases from ULSD to DBE20 but biodiesel has the highest BSVOF. Thus, at light load, due to the higher %VOF in the PM, the blended fuel leads to a higher VOF emission, while at high load the blended fuel leads to a reduction in both PM and VOF. The effect of high combustion temperature overrides the evaporation latent heat of ethanol and the oxygen conditions surrounding the blended fuel

http://dx.doi.org/10.5772/64470

benefit of the combustion such that the VOF component tends to decrease when the % ethanol in fuel increases up to 20%. Especially, BSVOF for biodiesel is the highest and ULSD is the second highest than that for other fuels. This is because biodiesel having more active surface pores and ULSD having higher concentrations of nucleated sulfur acid particles [42] for the condensation of VOF.

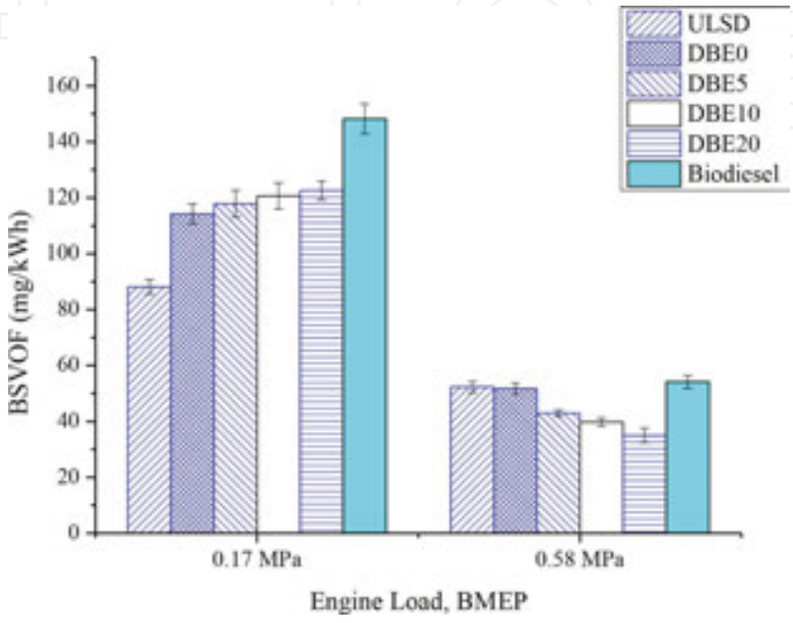

Figure 26. Variation of BSVOF with different fuels at two different engine loads.

7.2. Particle oxidative reactivity

The oxidation reactivity of combustion particles can be quantified by their soot ignition temperatures [43]. **Figure 27** shows the ignition temperature, at which the maximum heat flow rate occurs, of each fuel at the engine load of 0.58 MPa. It is the highest for ULSD (721.1°C) and the lowest for biodiesel (627.0°C), while for the blended fuels it decreases from 695.2 to 680.0°C with increased ethanol content from 0 to 20% in the fuel. In general, the ignition temperature decreases with the increase in the oxygen content in the fuel.

Based on the TGA data, a kinetic analysis was conducted on the oxidation of the nonvolatile fraction by using the Arrhenius plot of oxidation rates. **Table 10** shows the calculated kinetic parameters for particulate samples obtained from different fuels at the engine load of 0.58 MPa. The activation energy is the highest for diesel fuel and the lowest for biodiesel, while for the blended fuels it decreases with the increase in the ethanol content in the fuel. Thus, it decreases with increase in the oxygen content in the fuel. The lower the activation energy is, the higher the oxidative reactivity of the particulate sample will be [42]. Stanmore et al. [44] also reported that lower activation energy and higher reactivity could lead to lower ignition temperature. The above results indicate that the oxidative reactivity of particulates decreases in the order of biodiesel, DBE20, DBE10, DBE5, DBE0, and ULSD.

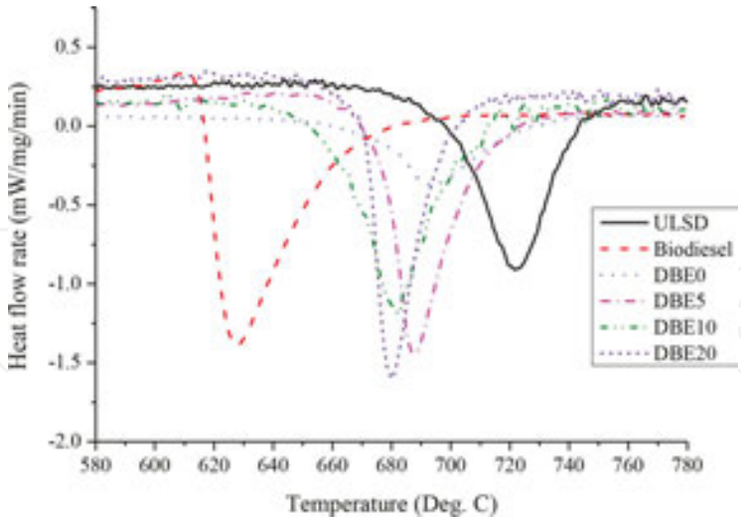

Figure 27. Heat flow rate (derivative of DSC signal) curves for different fuels at a high engine load of 0.58 MPa.

Fuels	BMEP (MPa)	Oxygen content (%)	Ignition temperature (°C)	Calculated activation energy (kJ/mol)	Calculated frequency factor (Sec^{-1})
ULSD	0.58	0.0	721.10	166.30	2.39E+08
DBE0	0.58	1.7	695.20	137.13	3.12E+07
DBE5	0.58	3.3	689.41	116.90	1.33E+07
DBE10	0.58	5.0	683.54	109.10	9.42E+06
DBE20	0.58	8.2	680.04	81.43	1.12E+06
Biodiesel	0.58	10.8	627.02	65.20	4.44E+05

Table 10. Calculated kinetic parameters of particulate samples of different fuels.

Particle volatility also affects the oxidation process. During the initial TGA thermal treatment from room temperature to 380°C, volatile fractions of test fuels filled inside the micropores of soot aggregates are removed under the argon environment. More internal particle surface areas are therefore available for subsequent soot oxidation. As such, higher %VOF would contribute higher reactivity and oxidation rate of particulates.

8. Transmission electron microscope analysis

This section is to investigate the particulate volatility and oxidation by a thermogravimetric analysis and morphology by transmission electron microscope analysis on a four-cylinder DI diesel engine using DBE blends with ethanol addition of 0, 5, 10, and 20% tested at a steady speed of 1800 rev/min under low and high engine loads of 0.17 and 0.58 MPa, respectively.

http://dx.doi.org/10.5772/64470

8.1. Properties of diesel agglomerates

The measurement of agglomerates includes maximum projected length (L) and maximum projected width normal to length (W) and projected primary particle diameter (D) and primary particle area (A). **Figures 28–33** shows the soot agglomerates produced from ULSD, biodiesel and DBE blends at the engine loads of 0.17 and 0.58 MPa, respectively. Agglomerates from different fuels at different loads were found to be composed of fine primary particles forming a mixture of chain-like structures and clusters of spherules. **Table 11** summarizes the above measurements of the soot agglomerates and their respective primary particles. For each fuel, the projected diameter and area of primary particles increase with engine load because more fuel is burned at higher load resulting in the growth of soot nuclei. The projected primary particle diameter increases in the order of DBE20 (15–18 nm), DBE10 (17–20 nm), DBE5 (19–23 nm), DBE0 (20–24 nm), biodiesel (24–31 nm), and ULSD (34–41 nm). The DBE blends, compared with biodiesel and diesel, produced smaller primary particles. Increasing the proportion of ethanol from DBE5 to DBE20, the carbon content of the blend fuels decreases and the oxygen content increases leading to the reduction of soot nuclei. The possibility of agglomeration and condensation of smaller particles to form larger ones is then reduced, leading to smaller agglomerates and primary particles. In this study, increasing ethanol from 5 to 20%, the projected length of agglomerates from DBE blends decreases from 448 to 419 nm at 0.17 MPa and 508 to 449 nm at 0.58 MPa while the projected width decreases from 562 to 387 nm at 0.17 MPa and 625 to 415 nm at 0.58 MPa.

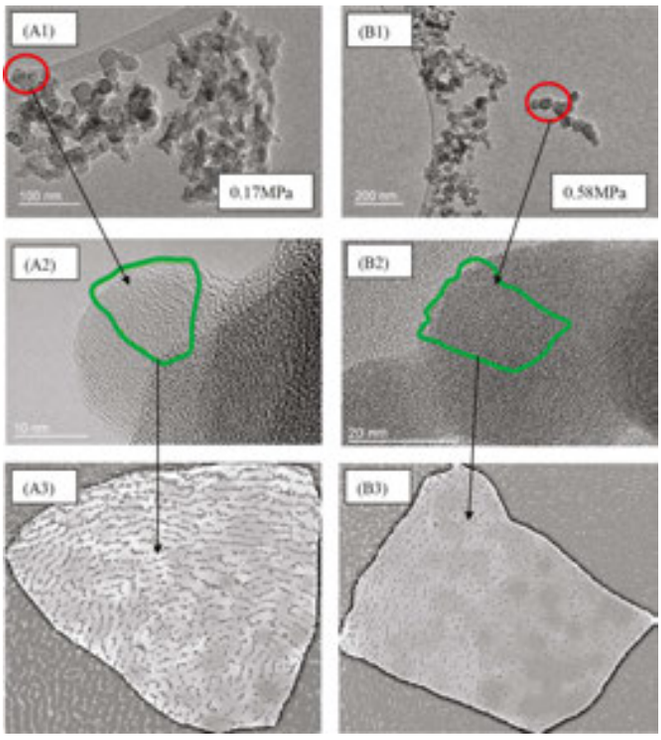

Figure 28. ULSD-derived primary particles at loads of 0.17 and 0.58 MPa: (1) TEM image, (2) high-magnified TEM image for ROIs, and (3) skeletonized ROI images.

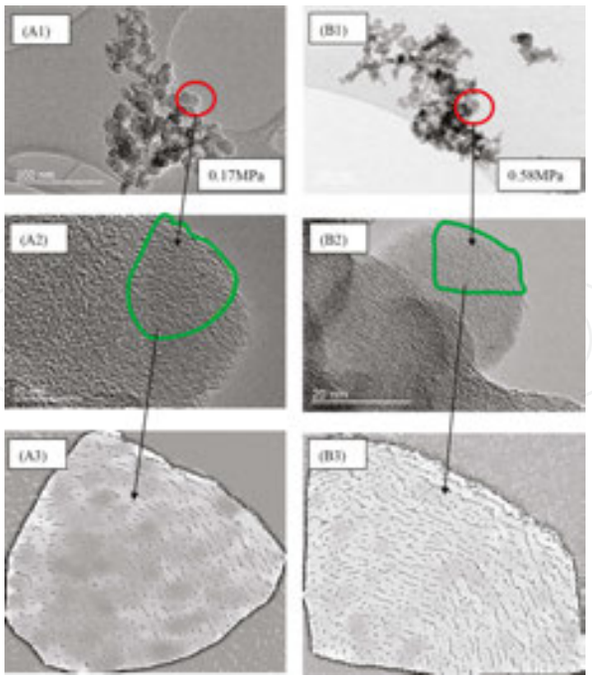

Figure 29. Biodiesel-derived primary particles at loads of 0.17 and 0.58 MPa: (1) TEM image, (2) high-magnified TEM image for ROIs, and (3) skeletonized ROI images.

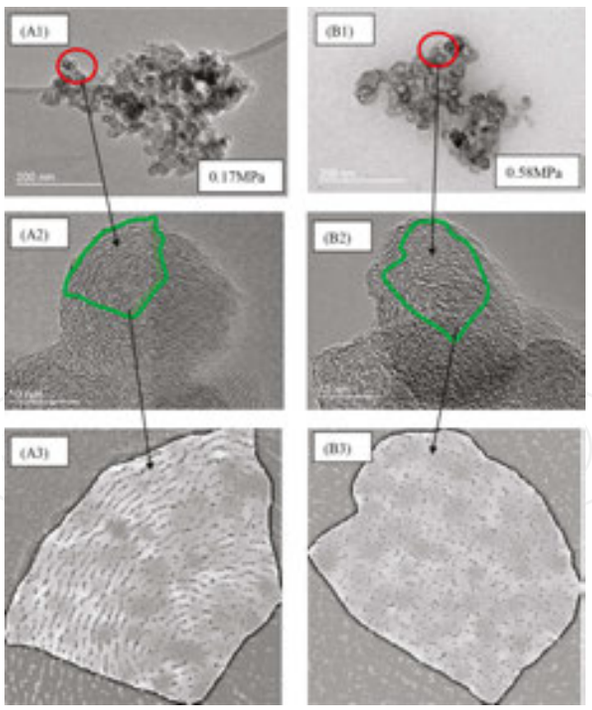

Figure 30. DBE0-derived primary particles at loads of 0.17 and 0.58 MPa: (1) TEM image, (2) high-magnified TEM image for ROIs, and (3) skeletonized ROI images.

http://dx.doi.org/10.5772/64470

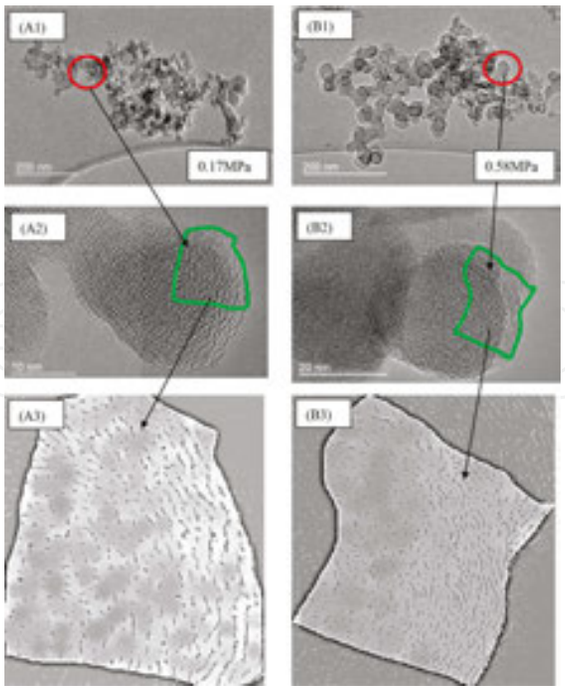

Figure 31. DBE5-derived primary particles at loads of 0.17 and 0.58 MPa: (1) TEM image, (2) high-magnified TEM image for ROIs, and (3) skeletonized ROI images.

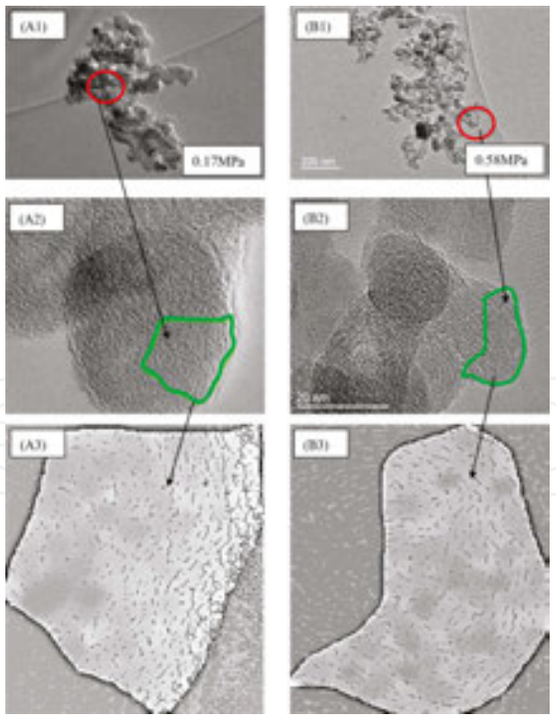

Figure 32. DBE10-derived primary particles at loads of 0.17 and 0.58 MPa: (1) TEM image, (2) high-magnified TEM image for ROIs, and (3) skeletonized ROI images.

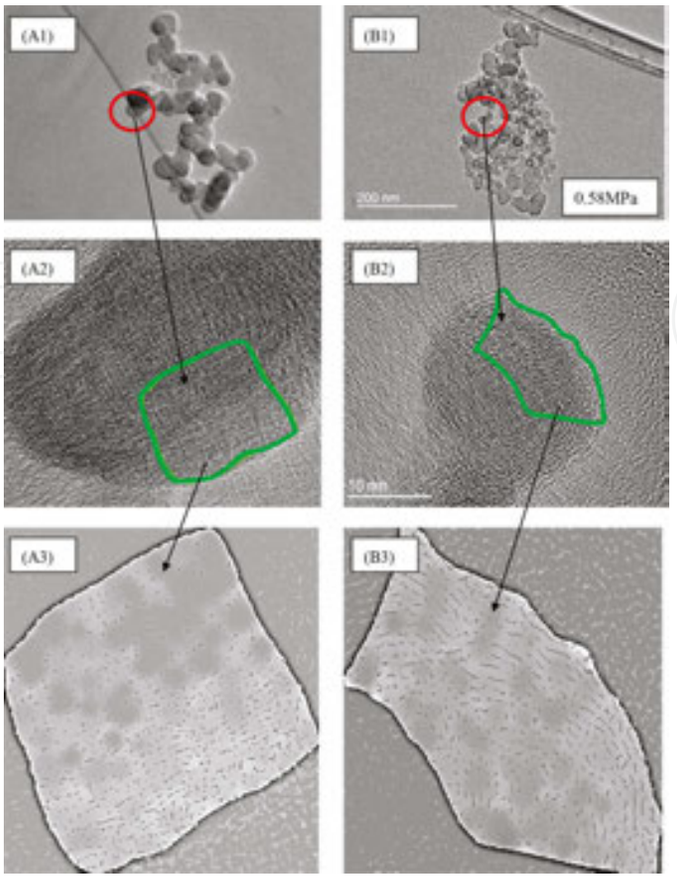

Figure 33. DBE20-derived primary particles at loads of 0.17 and 0.58 MPa: (1) TEM image, (2) high-magnified TEM image for ROIs, and (3) skeletonized ROI images.

8.2. Properties of fine particle nanostructures

For individual primary particle, the examination of its structure and distribution of graphene layers provide information about its nanostructure morphology. The classic core-shell structure of a primary particle from diesel fuel has an outer shell composed of planar-shaped crystallites oriented perpendicular to the radius of the particle and an inner core constituted by several fine spherules at the central portion. Other authors found different internal structures of diesel particles subject to different thermal exposure including (a) fullerenoid or onion-like morphology, (b) turbostratic graphite structures formed by small plates of undefined orientation, (c) purely turbostratic layers, and (d) structures formed by multiple spherical nuclei surrounded by several graphitic layers [19, 45–47]. The nanostructure can be further characterized and quantified by the fringe length, fringe separation, and tortuosity [48]. Variation in these parameters indicates different carbon nanostructures such as graphitic, fullerenic, and amorphous. HRTEM images at a high-magnification level in **Figure 28(A2)** and **(B2)** to **Figure 33(A2)** and **(B2)** show different morphology for fine primary particles from ULSD and biodiesel and DBE blends at engine loads of 0.17 and 0.58 MPa, respectively. Selected region of interest (ROI) on each image was processed and the skeletonized ROI binary images converted from **Figure 28(A1)** and **(B1)** to **Figure 33(A1)** and **(B1)** are shown in **Figure 28(A3)**

http://dx.doi.org/10.5772/64470

and **(B3)** to **Figure 33(A3)** and **(B3)**, respectively. They are further used to evaluate the nanostructure characteristics such as fringe length, fringe separation and, tortuosity. **Table 12** summarizes the measurements obtained by lattice fringe analysis, following the procedures in Vander Wal et al. [48] and Shim et al. [49].

Fuels	Load (MPa)	Figures	Numbers of agglomerates	$L_{average}$ (nm)	$W_{average}$ (nm)	$(L/W)_{average}$	Numbers of particles	$D_{average}$ (nm)	$A_{average}$ (nm^2)
ULSD	0.17	**Figure 28 (A1)**	4	241±23	303±45	0.8±0.3	39	34±4	942±29
Biodiesel	0.17	**Figure 29 (A1)**	4	488±48	424±56	1.3±0.4	35	24±4	485±32
DBE0	0.17	**Figure 30 (A1)**	4	360±23	363±20	0.9±0.3	43	20±3	332±29
DBE5	0.17	**Figure 31 (A1)**	4	448±75	562±52	0.9±0.4	52	19±3	300±24
DBE10	0.17	**Figure 32 (A1)**	4	434±54	417±23	1.0±0.2	47	17±5	224±15
DBE20	0.17	**Figure 33 (A1)**	4	419±68	387±41	1.1±0.3	46	15±4	172±17
ULSD	0.58	**Figure 28 (B1)**	4	275±50	373±33	1.0±0.4	29	41±7	1332±12
Biodiesel	0.58	**Figure 29 (B1)**	4	735±57	790±81	0.9±0.3	45	31±3	749±21
DBE0	0.58	**Figure 30 (B1)**	4	459±74	690±65	0.7±0.2	33	24±3	471±13
DBE5	0.58	**Figure 31 (B1)**	4	508±76	625±51	0.8±0.2	49	23±3	417±15
DBE10	0.58	**Figure 32 (B1)**	4	506±61	487±38	1.1±0.1	44	20±4	343±20
DBE20	0.58	**Figure 33 (B1)**	4	449±98	415±41	1.2±0.4	42	18±2	244±19

Table 11. Measurement of the soot agglomerates and their respective primary particles.

In general, the high-engine-load particulate samples for each test fuel exhibit more ordered and clear graphitic structures when compared with low-engine-load samples. At low engine load, particulate samples examined under the TEM micrographs are more amorphous and disordered due to their high content of volatile organic substances in the samples, which is in line with the findings from Lu et al. [42]. While increasing engine load with higher exhaust temperature, volatile organic substances in the samples are burnt out and the particles are then distinct and graphitic in morphology. Zhu et al. [20] in their study reported similar results that crystallite dimension of diesel particulate increases with engine load and exhaust temperature on a light-duty diesel engine.

For ULSD-derived soot, the primary particles possess typical shell-core structures and concentric ring patterns as shown in **Figure 28**. With an increase in the engine load from 0.17 to 0.58 MPa, the mean fringe length increases from 1.012 to 1.075 nm, the mean tortuosity is approximately in the range of 1.077–1.079 signifying that the fringes are not highly curved, and the mean fringe separation decreases from 0.414 to 0.336 nm. For biodiesel-derived soot, the primary particles possess long-range layers concentrically arranged along the outermost

periphery and short layers amorphously inside the inner as shown in **Figure 29**. When the engine load is increased from 0.17 to 0.58 MPa, the mean fringe length increases from 0.658 to 0.859 nm, the mean tortuosity decreases significantly from 1.117 to 1.111, indicating that the curvature of fringes slightly weakens under high load condition and the mean fringe separation is approximately in the range of 0.182–0.191 nm.

Fuels	Load (MPa)	Figures	Fringe length (nm)	Fringe separation (nm)	Tortuosity
ULSD	0.17	**Figure 28 (A3)**	1.012 ± 0.032	0.414 ± 0.012	1.079 ± 0.032
Biodiesel	0.17	**Figure 29 (A3)**	0.658 ± 0.079	0.191 ± 0.009	1.117 ± 0.040
DBE0	0.17	**Figure 30 (A3)**	0.969 ± 0.029	0.359 ± 0.023	1.107 ± 0.039
DBE5	0.17	**Figure 31 (A3)**	0.950 ± 0.020	0.350 ± 0.001	1.109 ± 0.042
DBE10	0.17	**Figure 32 (A3)**	0.903 ± 0.049	0.335 ± 0.022	1.111 ± 0.027
DBE20	0.17	**Figure 33 (A3)**	0.836 ± 0.078	0.320 ± 0.011	1.114 ± 0.009
ULSD	0.58	**Figure 28 (B3)**	1.075 ± 0.012	0.336 ± 0.014	1.077 ± 0.030
Biodiesel	0.58	**Figure 29 (B3)**	0.859 ± 0.067	0.182 ± 0.032	1.111 ± 0.038
DBE0	0.58	**Figure 30 (B3)**	1.033 ± 0.061	0.331 ± 0.019	1.068 ± 0.041
DBE5	0.58	**Figure 31 (B3)**	0.999 ± 0.041	0.345 ± 0.021	1.105 ± 0.014
DBE10	0.58	**Figure 32 (B3)**	0.987 ± 0.051	0.204 ± 0.031	1.078 ± 0.033
DBE20	0.58	**Figure 33 (B3)**	0.947 ± 0.071	0.289 ± 0.024	1.108 ± 0.037

Table 12. Measurement of the nanostructure characteristics.

For DBE-derived soot, fullerenic-like nanostructures are observed in **Figures 30–33**. The soot particles possess spherical buckyballs in center surrounded by the outer graphitic structures. For each blended fuel, increasing engine load increases the mean fringe length but decreases the tortuosity and fringe separation distance. With increasing ethanol contents in the blended fuels, the lamellae are more curved, tortuous, and disorganized. With ethanol addition from 0 to 20%, the mean fringe length reduces from 0.969 to 0.836 nm at 0.17 MPa and from 1.033 to 0.947 nm at 0.58 MPa. As compared with ULSD, DBE blends have lower mean fringe lengths reflecting more amorphous nanostructure while biodiesel has the least mean fringe lengths. The curvature of fringes for DBE blends increases with ethanol addition in particular under low load condition with mean tortuosity of 1.107–1.114 at 0.17 MPa. As for the mean fringe separation distance, ethanol addition has only mild effect and it decreases from 0.359 to 0.320 nm at low load and from 0.331 to 0.289 nm at high load.

Vander Wal et al. [22] reported that amorphous or fullerenic structured soots produced from oxygenated fuels would oxidize faster than graphitic structured soot from conventional diesel fuel thus producing less soot from tailpipe. The increase of tortuosity reflects the more amorphous structures produced from the soot. Tortuosity increases fringe separation such that adjacent carbon layer planes are more separated and more oxygen can access to the highly reactive edge-site carbon for oxidation. Song et al. [50] reported that the more amorphous arrangement within the particles reflected the more edge-site carbon density.

http://dx.doi.org/10.5772/64470

By combining the particulate emissions, and TGA and TEM results, the effects of engine load and fuel oxygenation on particle characteristics can be summarized. For the effect of engine load, it is found from all tested fuels that increasing load can lead to higher BSPM and BSPN emissions with larger primary particles formed but with lower BSVOF emissions. Under high combustion temperature at high load, the primary particles of all fuels exhibit more distinct structures as a consequence of the burnout VOFs. For all fuels, the mean fringe length decreases, and the mean fringe separation and tortuosity increase with the increase in the engine load except for the fringe length of DBE20 and tortuosity of ULSD which are not significantly influenced. Therefore, the engine load affects not only particulate mass-number emissions but also the graphitization of primary particles. For the effect of fuel oxygenation, it is generally found that with higher oxygen content in the fuel, the particulates would have larger percentage of VOF, lower soot burnout temperature (low activation energy), stronger oxidative reactivity, smaller primary particles, and more curved, tortuous, and disorganized nanostructures.

In general, the oxidative reactivity of particulates decreases in the order of biodiesel, DBE20, DBE10, DBE5, DBE0, and ULSD. Therefore, fuel oxygenation has more significant effect on reducing soot burnout temperature, lowering resistance to oxidation, and shifting toward more amorphous structures, thereby affecting particle volatility, oxidation, and morphology.

9. Conclusions

The performance of current available engine technologies is almost close to the statutory emission limits. In recent years, there has been an increase in fuel-change researches worldwide on use of transport biofuels such as biodiesel and alcohol to reduce engine emissions and fuel consumption as supplement measures without any engine modification works. In this study, engine experiments are performed with diesel-biodiesel blended with 0, 5, 10, and 20% ethanol with intake CO_2 ranging from 0 to 4.5%, at 1.5% interval, in a four-cylinder naturally aspirated DI engine tested at 1800 rev/min under different engine loads.

Engine performance, combustion characteristics, gaseous emissions, and particulate morphology are evaluated for assessing diesel-biodiesel-ethanol (DBE) blends as future fuel-change technology for using these three fuels efficiently, reducing engine emissions and minimizing reliance on diesel fuel. Each experimental test is repeated three times to ensure that the results are repeatable within the experimental uncertainties. Student's *t*-test is employed to analyze whether the difference between the results obtained from different test fuels are statistically significant at the 95% confidence level. The main conclusions from this study are drawn as follows:

1. DBE blends can effectively reduce the emissions of NO_x and C_{O2}, and PM and total particle number concentration of all sizes but lead to an increase of CO and HC emissions in low engine loads which could be resolved using diesel oxidation catalytic converter. The use of DBE facilitates the effective use of diesel-biodiesel blended fuels with improved fuel quality and reduced emissions, in particular for NO_x and PM, without the need for engine

modification. On engine performance, brake-specific fuel consumption increases with ethanol in DBE blends and the increases slightly due to improved brake thermal efficiency (BTE) at high engine loads. BTE also increases with ethanol, but again increases slightly when cooling effects of ethanol are nullified with the high in-cylinder gas temperature at high engine loads. From low to medium engine loads, the in-cylinder pressure curve of DBE blends shifts away from top dead center to the right when increasing ethanol contents. But at high loads, there is no significant change in the cylinder pressure rise with ethanol addition as a result of the shortened ignition delay period and consequently less fuel accumulates and burns in the premixed phase.

2. DBE blends have comparatively higher oxygen content, lower carbon content, and lower diffusion fuel mass than ultra-low-sulfur diesel (ULSD). Increasing ethanol fractions in DBE blends, cetane number decrease leading to longer ignition delay and shorter combustion duration. The improved combustion with more oxygen contents and lower diffusion fuel mass from DBE blends enhance the reductions of brake-specific particulate mass (BSPM) and particle number (BSPN) emissions. The application of DBE blends can attain lower BSPM and BSPN emissions in particular with lesser ultrafine and nanoparticle concentrations than ULSD. On the contrary, biodiesel led to increase of total particle, ultrafine, and nanoparticle concentrations.

3. CO_2 is used to dilute the intake air of a four-cylinder DI diesel engine fueled by DBE blends to reduce NO_x while minimizing the adverse impact on particulate emissions at high engine load. The results include brake-specific fuel consumption, brake thermal efficiency, combustion characteristics, brake-specific NO_x, brake-specific PM mass, and particle number emissions for diesel-biodiesel blended with 5, 10, and 20% ethanol with intake CO_2 of 1.5, 3, and 4.5% tested at a steady speed of 1800 rev/min under a high engine load of 0.58 MPa. It is found that combined effect of DBE blends with intake CO_2 dilution has marginal effects on brake-specific fuel consumption and brake thermal efficiency, which significantly reduces NO_x emission while slightly increases particulate emissions.

4. The test of thermogravimetric analysis shows that higher percentage of volatile organic fractions (VOF) in fuel will lead to higher reactivity and oxidation rate of particles due to more internal particle surface areas left from the lost VOF for soot oxidation. DBE blends are found oxidized faster with lower activation energy at lower ignition temperature than ULSD while oxidized slower than biodiesel. The oxidative reactivity of particles increases in order of ULSD, DBE0, DBE5, DBE10, DBE20, and biodiesel.

5. Internal nanostructure morphology of soot governs the particle oxidative reactivity. Agglomerates from different fuels are found to be composed of fine primary particles forming a mixture of chain-like structures and clusters of spherules. Increasing the fuel oxygenation leads to the increase of amorphous nanostructure characterized by smaller particle size, shorter and curved fringe-length distribution, shorter fringe separation, and higher tortuosity. Increasing the ethanol contents in DBE blends, the lamella becomes more curved, tortuous, and disorganized. The reactivity of DBE blends is generally higher than ULSD. However, the high oxygen and VOF contents in biodiesel are the major reasons

http://dx.doi.org/10.5772/64470

for its highest reactivity among the test fuels though its fringe length and tortuosity are longer and lower respectively than DBE blends.

Overall, it is concluded that the use of DBE blends can effectively reduce the NO_x, CO_2, total particle numbers with lesser ultrafine and nanoparticle concentrations than ULSD, and neat biodiesel except particulate mass concentrations a bit higher than biodiesel. By supplementing with limited intake CO_2 charge dilution, the reduction of NO_x can be further enhanced but particulate mass emissions are slightly increased.

The experimental results in this study could be applied directly in those countries with diesel engines and diesel fuel sulfur levels similar to the test Euro 2 engine and 50 ppm containing ULSD used in this study. While for those countries with newer technology-based diesel engines or lower sulfur-containing diesel fuels, the experimental results could be served as the reference data, but mapping work with revalidation test on engine performance, combustion characteristics, and emission performance is required when using DBE blends as transport biofuels.

Nomenclature

CO_2	Carbon dioxide
CO	Carbon monoxide
DBE	Diesel-biodiesel-ethanol blends
HC	Hydrocarbons
NO_2	Nitrogen dioxide
NO_x	Nitrogen oxides
PM	Particulate matters
PN	Particle number concentrations
ULSD	Ultra-low-sulfur diesel
HFID	Heated flame ionization detector
HCLA	Heated chemiluminescence analyzer
TEOM	Tapered element oscillating microbalance
NDIR	Nondispersive infrared analyzer
SMPS	Scanning mobility particle sizer
TGA	Thermogravimetric analysis
BMEP	Brake mean effective pressure
BSFC	Brake-specific fuel consumption
BTE	Brake thermal efficiency
SOC	Start of combustion

EOC	End of combustion
BSCO	Brake-specific CO emissions
$BSCO_2$	Brake-specific CO_2 emissions
BSHC	Brake-specific hydrocarbon emissions
$BSNO_x$	Brake-specific nitrogen oxide emissions
BSPM	Brake-specific particulate mass emissions
BSPN	Brake-specific particle number emissions
SOC	Start of combustion
EOC	End of combustion
TDC	Top dead center
LHV	Lower heating value
VOF	Volatile organic fraction
HRTEM	High-resolution transmission electron microscope
ROI	Region of interest
Øp	Premixed combustion phase
Ød	Diffusion combustion phase

Author details

Ho Tse

Address all correspondence to: jeff.tse@connect.polyu.hk

The Hong Kong Polytechnic University, Hong Kong, China

References

[1] Ribeiro NM, Pinto AC, Quintella CM, Rocha GO, Teixeira LSG, Guaririro LLN, Rangel MDC, Veloso MCC, Renzende MJC, Cruz RS, Oliveira AM, Torres EA, Andrade JB, "The role of additives for diesel and diesel blended (ethanol or biodiesel) fuels: a review", Energy & Fuels, 21, 2007.

[2] Cheung CS, Cheng C, Chan TL, Lee SC, Yao C, Tsang KS, "Emission characteristics of a diesel engine fuelled with biodiesel and fumigation methanol", Energy & Fuels, 22, 906–914, 2008.

[3] Agarwal AK, "Biofuels (alcohols and biodiesel) applications as fuels for internal combustion engines", Progress in Energy and Combustion Science, 33, 233–271, 2007.

http://dx.doi.org/10.5772/64470

[4] Demirbas A, "Progress and recent trends in biofuels", Progress in Energy and Combustion Science 33, 1–18, 2007.

[5] Kumar S, Cho JH, Moon Park J, Moon II, "Advances in diesel-alcohol blends and their effects on the performance and emissions of diesel engines", Renewable and Sustainable Energy Reviews, 22, 46–72, 2013.

[6] Kuchler M, Linner BO, "Challenging the food vs fuel dilemma: genealogical analysis of the biofuel discourse pursued by international organization", Food Policy, 37, 581–588, 2012.

[7] Thompson PB, "The agricultural ethics of biofuels: the food vs fuel debate", Agriculture, 2, 339–358, 2012.

[8] Lapuerta M, Agudelo JR, Armas O, "Effect of biodiesel fuels on diesel engine emissions", Progress in Energy and Combustion Science, 34, 198–223, 2008.

[9] David YC, Chang Jon H Van Gerpen, "Determination of particulate and unburned hydrocarbon emissions from diesel engines fueled with biodiesel", SAE Technical Paper Series 982527, 1998.

[10] Dorado MP, Ballesteros E, Arnal JM, Gomez J, Lopez FJ, "Exhaust emissions from a diesel engine fueled with transesterified waste olive oil", Fuel, 82, 1311–1315, 2003.

[11] Ramadhas AS, Muraleedharan C, Jayaraj S, "Performance and emission evaluation of a diesel engine fueled with methyl esters of rubber seed oil", Renewable Energy, 30, 1789–1800, 2005.

[12] Peng CY, Yang HH, Lan CH, Chien SM, "Effects of the biodiesel blend fuel on aldehyde emissions from diesel engine exhaust", Atmospheric Environment, 42, 906–915, 2008.

[13] Di Y, Cheung CS, Huang Z, "Experimental investigation on regulated and unregulated emissions of a diesel engine fueled with ULSD blended with biodiesel from waste cooking oil", Science of the Total Environment, 407, 835–846, 2009.

[14] Song KH, Nag P, Litzinger TA, "Effects of oxygenated additives on aromatic species in fuel-rich, premixed ethane combustion: a modeling study" Combustion Flame, 135, 341–349, 2003.

[15] Sayin C, "Engine performance and exhaust gas emissions of methanol and ethanol-diesel blends", Fuel, 89, 3410–3415, 2010.

[16] Zhu L, Cheung CS, Zhang WG, Huang Z, "Emission characteristics of a diesel engine operating on biodiesel and biodiesel blended with ethanol and methanol", Science of the Total Environment, 408, 914–921, 2010.

[17] Di Y, Cheung CS, Huang Z, "Experimental study on particulate emission of a diesel engine fueled with blended ethanol-dodecanol-diesel", Aerosol Science, 40, 101–112, 2009.

[18] Cinar C, Topgul T, Ciniviz M, Hasimoglu C, "Effects of injection pressure and intake CO_2 concentration on performance and emission parameters of an IDI turbocharged diesel engine", Applied Thermal Engineering, 25, 1854–1862, 2005.

[19] Chen Y, Shah N, Braun A, Huggins FE, Huffman GP, "Electron microscopy investigation of carbonaceous particulate matter generated by combustion of fossil fuels", Energy & Fuels, 19, 1644–1651, 2005.

[20] Zhu J, Lee KO, Yozgatligil A, Choi MY, "Effects of engine operating conditions on morphology, microstructure and fractal geometry of light-duty diesel engine particulates", Proceedings of the Combustion Institute, 30, 2781–2789, 2005.

[21] Rakopoulos DC, Rakopoulous CD, Giakoumis EG, Dimaratos AM, "Characteristics of performance and emissions in high-speed direct injection diesel engine fuelled with diethyl ether/diesel fuel blends", Energy, 43, 214–224, 2012.

[22] Vander Wal RL, Mueller, CJ. "Initial investigation of effects of fuel oxygenation on nanostructure of soot from a direct-injection diesel engine", Energy & Fuels, 20, 2364–2369, 2006.

[23] SAE International, "Test procedure for the measurement of gaseous exhaust emissions from small utility engines", SAE International Paper J1088, 2003.

[24] Moffat RJ, "Describing the uncertainties in experimental results", Experimental Thermal and Fluid Science, 1, 3–7, 1998.

[25] Shi X, Yu Y, He H, Shuai S, Dong H, Li R, "Combination of biodiesel-ethanol-diesel fuel blend and SCR catalyst assembly to reduce emissions from a heavy-duty diesel engine", Journal of Environment Sciences, 20, 177–182, 2008.

[26] Qi DH, Chen H, Geng LM, Bian Y ZH, Ren X CH, "Performance and combustion characteristics of biodiesel-diesel-methanol blend fuelled engine", Applied Energy, 87, 1679–1686, 2010.

[27] Zhu L, Cheung CS, Zhang WG, Huang Z, "Combustion, performance and emission characteristics of a DI diesel engine fueled with ethanol-biodiesel blends", Fuel, 90, 1743–1750, 2011.

[28] Boehman AL, Morris D, Szybist JP, Esen E, "The impact of the bulk modulus of diesel fuels on fuel injection timing", Energy & Fuels, 18, 1877–1882, 2004.

[29] Szybist JP, Song J, Alam M, Boehman AL, "Biodiesel combustion, emissions and emission control", Fuel Processing Technology, 88, 679–691, 2007.

[30] Sivalakshmi S, Balusamy T, "Effects of dimethylcarbonate-biodiesel blends on the combustion, performance and exhaust emissions of a DI diesel engine", SAE International, 2012.

[31] Kwanchareon P, Luengnaruemitchai A, Jai-Lin S, "Solubility of a diesel-biodiesel-ethanol blend, its fuel properties, and its emission characteristics from diesel engine", Fuel, 86, 1053–1061, 2007.

[32] Jha SK, Fernando S, Columbus E, Willcutt H, "A comparative study of exhaust emissions using diesel-biodiesel-ethanol blends in new and used engines", Transactions of the ASABE, 52, 375–381, 2009.

[33] Labecki L, Lindner A, Winklmayr W, Uitz R, Cracknell R, Ganippa L, "Effects of injection parameters and EGR on exhaust soot particle number-size distribution for diesel and RME fuels in HSDI engines", Fuel, 112, 224–235, 2013.

[34] Tree DR, Svensson KI, "Soot processes in compression ignition engines", Progress in Energy and Combustion Science, 33, 272–309, 2007.

[35] Leung DYC, Luo Y, Chan TL, "Optimization of exhaust emissions of a diesel engine fuelled with biodiesel", Energy & Fuels, 20, 1015–1023, 2006.

[36] Tan P, Lou D, Hu Z, " Nucleation mode particle emissions from a diesel engine with biodiesel and petroleum diesel fuels", SAE Technical Paper 2010-01-0787, 2010.

[37] Tsolakis A, "Effects on particle size distribution from the diesel engine operating on RME-biodiesel with EGR", Energy & Fuels 2006, 20, 1418–1424, 2006.

[38] Pang J, "Study of particle size distributions emitted by a diesel engine", SAE Technical Paper Series 1999-01-1141, 1999.

[39] Hulwan DB, Joshi SV, "Performance, emission and combustion characteristic of a multicylinder DI diesel engine running on DBE blends of high ethanol content", Applied Energy, 80, 5042–5055, 2011.

[40] Tse H, Leung CW, Cheung CS, "Engine performance and emissions of diesel-biodiesel-ethanol blend fuelled engine", International Conference on Applied Energy ICAE 2012, ICAE2012-A10789, 2012.

[41] Ladommatos N, Abdelhalim S, Zhao H, "Control of oxides of nitrogen from diesel engines using diluents while minimizing the impact on particulate pollutants", Applied Thermal Engineering, 18, 963–980, 1998.

[42] Lu T, Cheung CS, Huang Z, "Investigation on particle oxidation from a DI diesel engine fuelled with three fuels", Aerosol Science and Technology, 12, 46, 1349–1358, 2012.

[43] Stratakis GA, Stamatelos AM, "Thermogravimetric analysis of soot emitted by a modern diesel engine run on catalyst-doped fuel", Combustion and Flame, 132, 157–169, 2003.

[44] Stanmore BR, Brihac JF, Gilot P, "The oxidation of soot: a review of experiments, mechanisms and models", Carbon, 39, 2247–2268, 2001.

[45] Ishiguro T, Takatori Y, Akihama K, "Microstructure of diesel soot particles probed by electron mircroscopy: first observation of inner core and outer shell", Combustion and Flame, 108, 231–234, 1997.

[46] Wentzel M, Gorzawski H, Naumann KH, Saathoff H, Weinbrush S, "Transmission electron microscopical and aerosol dynamical characterization of soot aerosols", Journal of Aerosol Science, 34, 1347–1370, 2003.

[47] Lipkea WH, Johnson JH, Vuk CT, "The physical and chemical character of diesel particulate emissions—measurement techniques and fundamental considerations", SAE Paper 780108, 1978.

[48] Vander Wal RL, Tomasek AJ, Pamphlet MI, Taylor CD, Thompson WK, "Analysis of HRTEM images for carbon nanostructure quantification", Journal of Nanoparticle Research, 6, 555–568, 2004.

[49] Shim HS, Hurta RH, Yang NYC, "A methodology for analysis of 002 lattice fringe images and its application to combustion-derived carbons", Carbon, 38, 29–45, 2000.

[50] Song J, Alam M, Boehman AL, Kim U, "Examination of the oxidation behavior of biodiesel soot", Combustion and Flame, 146, 589–604, 2006.